

Study on muon MDM and lepton EDM in BLMSSM via the mass insertion approximation

Xi Wang^{1,2,3*}, Shu-Min Zhao^{1,2,3†}, Xin-Xin Long^{1,2,3},
Yi-Tong Wang^{1,2,3}, Tong-Tong Wang^{1,2,3}, Hai-Bin
Zhang^{1,2,3}, Tai-Fu Feng^{1,2,3,4}, Rong-Xiang Zhang^{1,2,3‡}

¹ *Department of Physics, Hebei University, Baoding, 071002, China*

² *Hebei Key Laboratory of High-precision Computation and
Application of Quantum Field Theory, Baoding, 071002, China*

³ *Research Center for Computational Physics
of Hebei Province, Baoding, 071002, China and*

⁴ *Department of Physics, Chongqing University, Chongqing 401331, China*

(Dated: March 7, 2023)

Abstract

In the framework of the MSSM extension with local gauged baryon and lepton numbers (BLMSSM), we calculate the muon anomalous magnetic dipole moment (MDM) and lepton (e, μ, τ) electric dipole moment (EDM), and discuss how the muon MDM and lepton EDM depend on the parameters within the mass insertion approximation. Among many parameters, $\tan \beta$, g_L , m_L and μ_H are more sensitive parameters for a_μ^{BL} . Considering the experimental limitations, our best numerical result of a_μ^{BL} is around 2.5×10^{-9} , which can well compensate the departure between the experiment data and Standard Model (SM) prediction. The CP violating phases in BLMSSM are more than those in the MSSM, including new parameters θ_{μ_L} and θ_L . They can give large contributions, which play an important role in exploring the source of CP violation and probing new physics beyond SM.

PACS numbers:

Keywords: Muon MDM, CP violation, Mass insertion approximation

* wx_0806@163.com

† zhaosm@hbu.edu.cn

‡ zrx@hbu.edu.cn

Contents

I. Introduction	1
II. The BLMSSM	3
III. Formulation	6
A. The muon MDM	6
1. The mass eigenstate	6
2. The mass insertion approximation	8
3. Degenerate result	10
B. The lepton EDM	11
IV. Numerical results	13
A. The relative error between the two methods	14
B. The muon MDM by MIA	14
1. One-dimensional graphs	15
2. Multidimensional scatter plots graphs	18
C. The lepton EDM by MIA	21
1. The electron EDM	21
2. The muon EDM	23
3. The tau EDM	25
V. Discussion and conclusion	25
Acknowledgments	26
References	27

I. INTRODUCTION

In the development of the Standard Model (SM), the muon anomalous magnetic dipole moment (MDM) is an urgent problem to be solved, which indicates that there must be new physics beyond SM. The muon MDM is denoted by $a_\mu \equiv (g_\mu - 2)/2$. The SM contributions to muon MDM have the following parts : 1. the QED loop contributions [1–15]; 2. the electroweak contributions [14, 15]; 3. the hadronic vacuum polarization contributions [1, 4, 16]; 4. the hadronic light-by-light contributions [10–12]. The specific expressions are as follows:

$$\begin{aligned} a_\mu^{QED} &= 116584718.931(104) \times 10^{-11}, \\ a_\mu^{EW} &= 153.6(1.0) \times 10^{-11}, \\ a_\mu^{HVP} &= 6845(40) \times 10^{-11}, \\ a_\mu^{HLBL} &= 92(18) \times 10^{-11}. \end{aligned} \tag{1}$$

Based on the above, SM prediction of muon anomaly is $a_\mu^{SM} = 116591810(43) \times 10^{-11}(0.37\text{ppm})$ [1, 8, 17, 18]. New result on the muon MDM is reported by the E989 collaboration at Fermilab [19]: $a_\mu^{FNAL} = 116592040(54) \times 10^{-11}(0.46\text{ppm})$ and 3.3 standard deviations larger than the SM prediction, which is in great agreement with BNL E821 result [2]. The new averaged experiment value of muon anomaly is $a_\mu^{exp} = 116592061(41) \times 10^{-11}(0.35\text{ppm})$. Combining all available measurements, we now obtain 4.2σ deviation between the experiment and SM expectation ($\Delta a_\mu = a_\mu^{exp} - a_\mu^{SM} = 251(59) \times 10^{-11}$).

The study of lepton electric dipole moment (EDM) is used to probe the source of CP violation [20]. The latest experiment shows that the upper bound of electron EDM is $|d_e^{exp}| < 1.1 \times 10^{-29}$ e.cm at the 90% confidence level [21–23], the muon EDM is $|d_\mu^{exp}| < 1.8 \times 10^{-19}$ e.cm at the 95% confidence level and the tau EDM is $|d_\tau^{exp}| < 1.1 \times 10^{-17}$ e.cm at the 95% confidence level [24]. The estimated SM value for the electron EDM is about $|d_e| \simeq 10^{-38}$ e.cm [25, 26], which is too small to be detected by the current experiments. Therefore, if large electron EDM is probed, one can ensure it is the sign of new physics beyond SM.

The study of muon MDM and lepton EDM has very important practical significance for exploring new physics. Some studies investigate the supersymmetric (SUSY) one-loop contributions to muon MDM. The authors [27, 28] obtain the approximate SUSY one-loop

contributions by simplification

$$|a_\mu^{SUSY}| = 13 \times 10^{-10} \left(\frac{100\text{GeV}}{M_{SUSY}} \right)^2 \tan \beta \text{sign}[\mu_H]. \quad (2)$$

Here, M_{SUSY} represents the masses of neutralinos, charginos and scalar leptons of the second generation, which are equal. The SUSY contributions can be easily evaluated from Eq. (2). The authors [29] study the muon g-2 in several GUT-scale constrained SUSY models, such as CMSSM/mSUGRA, pMSSM, CMSSM/mSUGRA extensions and GMSB/AMSB extensions. The numerical result of muon g-2 is researched with the MultiNest technique for the parameter space [30–32] in the GNMSSM with a singlino-dominated neutralino as a dark matter candidate. The muon g-2 is further studied under \mathbb{Z}_3 -NMSSM with LHC analyses in Ref. [33]. They study to what extent the g-2 can be explained in anomaly mediation scenarios [34]. Even if there is no new particle in this energy range, one can measure the g-2 directly via the channel to a Higgs boson and a monochromatic photon [35]. Next, let's briefly review our previous work on muon MDM. We study the corrections from loop diagrams to muon MDM with the mass eigenstate in the BLMSSM and B-LMSSM [36–38]. With the effective Lagrangian method [39–41], we also research the contributions to muon MDM from loop diagrams under the $U(1)_X$ SSM and $\mu\nu$ SSM.

To better explain the CP violation mechanism [42–45], scientists are trying to find CP violating terms in new physics beyond SM. In the MSSM [46–49], there are several CP violating phases, which can contribute significantly to the lepton EDM. The normal size CP violating phases $O(1)$ and particle mass in the TeV range can cause the electron EDM to exceed the current experimental upper limit ($|d_e^{exp}| < 1.1 \times 10^{-29}$ e.cm). In order to rectify this situation, there are three ways: the first is to make the phases small $O(10^{-2} - 10^{-3})$, the second is to increase the particle mass to the several 10 TeV range, and the third is to make internal cancellations between phases [50, 51].

In the extension of SM, the MSSM [46] is one of the most widely studied models. The authors propose the extension of the MSSM with local gauged B and L (BLMSSM) [52, 53], where the baryon and lepton numbers are local gauge symmetries spontaneously broken at the TeV scale. The BLMSSM has two advantages: one is that the broken baryon number (B) can explain asymmetry of matter-antimatter in the universe, and the other is that the broken lepton number (L) can generate tiny neutrino mass by the seesaw mechanism. In BLMSSM, the proton decay can be avoided by discrete symmetry called matter parity and

R-parity [54].

In this paper, we investigate the BLMSSM contributions to the muon MDM and lepton (e, μ, τ) EDM via the mass insertion approximation (MIA). In the process of analysis, we show the mass eigenstate expressions of muon MDM, the MIA expressions of muon MDM and lepton EDM in detail. We discuss the numerical difference between the mass eigenstate expressions and the MIA expressions to prove the accuracy of the latter. In comparison, the MIA makes it easier and more intuitive to observe sensitive parameters. However, in the BLMSSM, the one-loop corrections are similar to the MSSM results in analytic form. The difference is that the BLMSSM contributions have the new gaugino λ_L and gauge coupling constant g_L . Under the latest experimental constraints, our results can well enough compensate the deviation of muon MDM and satisfy the experimental limitations of lepton EDM.

The rest of the paper is organized as follows. In Section II, we briefly summarize the main components of the BLMSSM. In Section III, we show analytic forms of the BLMSSM contributions to the muon MDM (a_μ^{BL}) and the lepton EDM (d_l^{BL}). In Section IV, some numerical results are shown. The last section is devoted to summary.

II. THE BLMSSM

The local gauge group of BLMSSM is $SU(3)_C \otimes SU(2)_L \otimes U(1)_Y \otimes U(1)_B \otimes U(1)_L$ [55, 56]. Compared with MSSM, BLMSSM includes exotic quarks $(\hat{Q}_4, \hat{U}_4^c, \hat{D}_4^c, \hat{Q}_5^c, \hat{U}_5, \hat{D}_5)$ and exotic leptons $(\hat{L}_4, \hat{E}_4^c, \hat{N}_4^c, \hat{L}_5^c, \hat{E}_5, \hat{N}_5)$, which are used to eliminate B and L anomaly, respectively. The exotic Higgs $(\hat{\Phi}_B, \hat{\varphi}_B)$ are used to break B spontaneously with nonzero vacuum expectation values (VEVs), and the exotic Higgs $(\hat{\Phi}_L, \hat{\varphi}_L)$ are used to break L spontaneously with nonzero VEVs. The superfields \hat{X} and \hat{X}' are used to make the exotic quarks unstable. The right-handed neutrinos N_R^c are introduced to provide tiny masses of neutrinos through the seesaw mechanism. Table I displays these additional fields in detail.

In the BLMSSM, the superpotential is expressed as [57]

$$\mathcal{W}_{BLMSSM} = \mathcal{W}_{MSSM} + \mathcal{W}_B + \mathcal{W}_L + \mathcal{W}_X, \quad (3)$$

where, \mathcal{W}_{MSSM} is the superpotential of the MSSM. The concrete forms of $\mathcal{W}_B, \mathcal{W}_L, \mathcal{W}_X$ are

$$\mathcal{W}_B = \lambda_Q \hat{Q}_4 \hat{Q}_5^c \hat{\Phi}_B + \lambda_U \hat{U}_4^c \hat{U}_5 \hat{\varphi}_B + \lambda_D \hat{D}_4^c \hat{D}_5 \hat{\varphi}_B + \mu_B \hat{\Phi}_B \hat{\varphi}_B$$

TABLE I: The new fields in the BLMSSM.

Superfields	$SU(3)_C$	$SU(2)_L$	$U(1)_Y$	$U(1)_B$	$U(1)_L$
\hat{Q}_4	3	2	1/6	B_4	0
\hat{U}_4^c	$\bar{3}$	1	-2/3	$-B_4$	0
\hat{D}_4^c	$\bar{3}$	1	1/3	$-B_4$	0
\hat{Q}_5^c	$\bar{3}$	2	-1/6	$-(1 + B_4)$	0
\hat{U}_5	3	1	2/3	$1 + B_4$	0
\hat{D}_5	3	1	-1/3	$1 + B_4$	0
\hat{L}_4	1	2	-1/2	0	L_4
\hat{E}_4^c	1	1	1	0	$-L_4$
\hat{N}_4^c	1	1	0	0	$-L_4$
\hat{L}_5^c	1	2	1/2	0	$-(3 + L_4)$
\hat{E}_5	1	1	-1	0	$3 + L_4$
\hat{N}_5	1	1	0	0	$3 + L_4$
$\hat{\Phi}_B$	1	1	0	1	0
$\hat{\varphi}_B$	1	1	0	-1	0
$\hat{\Phi}_L$	1	1	0	0	-2
$\hat{\varphi}_L$	1	1	0	0	2
\hat{X}	1	1	0	$2/3 + B_4$	0
\hat{X}'	1	1	0	$-(2/3 + B_4)$	0
\hat{N}_R^c	1	1	0	0	-1

$$\begin{aligned}
 & +Y_{u_4}\hat{Q}_4\hat{H}_u\hat{U}_4^c + Y_{d_4}\hat{Q}_4\hat{H}_d\hat{D}_4^c + Y_{u_5}\hat{Q}_5^c\hat{H}_d\hat{U}_5 + Y_{d_5}\hat{Q}_5^c\hat{H}_u\hat{D}_5 , \\
 \mathcal{W}_L = & Y_{e_4}\hat{L}_4\hat{H}_d\hat{E}_4^c + Y_{\nu_4}\hat{L}_4\hat{H}_u\hat{N}_4^c + Y_{e_5}\hat{L}_5^c\hat{H}_u\hat{E}_5 + Y_{\nu_5}\hat{L}_5^c\hat{H}_d\hat{N}_5 \\
 & +Y_{\nu}\hat{L}\hat{H}_u\hat{N}^c + \lambda_{N^c}\hat{N}^c\hat{N}^c\hat{\varphi}_L + \mu_L\hat{\Phi}_L\hat{\varphi}_L , \\
 \mathcal{W}_X = & \lambda_1\hat{Q}\hat{Q}_5^c\hat{X} + \lambda_2\hat{U}^c\hat{U}_5\hat{X}' + \lambda_3\hat{D}^c\hat{D}_5\hat{X}' + \mu_X\hat{X}\hat{X}' .
 \end{aligned} \tag{4}$$

The local gauge symmetry $SU(3)_C \otimes SU(2)_L \otimes U(1)_Y \otimes U(1)_B \otimes U(1)_L$ can break down to the electromagnetic symmetry $U(1)_e$, when the $SU(2)_L$ doublets (H_u , H_d) and singlets (Φ_B , φ_B , Φ_L , φ_L) obtain nonzero VEVs v_u , v_d and v_B , \bar{v}_B , v_L , \bar{v}_L respectively. The $SU(2)_L$

doublets and singlets are shown as

$$\begin{aligned}
H_u &= \begin{pmatrix} H_u^+ \\ \frac{1}{\sqrt{2}}(v_u + H_u^0 + iP_u^0) \end{pmatrix}, & H_d &= \begin{pmatrix} \frac{1}{\sqrt{2}}(v_d + H_d^0 + iP_d^0) \\ H_d^- \end{pmatrix}, \\
\Phi_B &= \frac{1}{\sqrt{2}}(v_B + \Phi_B^0 + iP_B^0), & \varphi_B &= \frac{1}{\sqrt{2}}(\bar{v}_B + \varphi_B^0 + i\bar{P}_B^0), \\
\Phi_L &= \frac{1}{\sqrt{2}}(v_L + \Phi_L^0 + iP_L^0), & \varphi_L &= \frac{1}{\sqrt{2}}(\bar{v}_L + \varphi_L^0 + i\bar{P}_L^0).
\end{aligned} \tag{5}$$

The soft breaking terms of BLMSM are shown as follows [53, 55, 56]

$$\begin{aligned}
\mathcal{L}_{soft} &= \mathcal{L}_{soft}^{MSSM} - (m_{\tilde{\nu}^c}^2)_{IJ} \tilde{N}_I^{c*} \tilde{N}_J^c - m_{\tilde{Q}_4}^2 \tilde{Q}_4^\dagger \tilde{Q}_4 - m_{\tilde{U}_4}^2 \tilde{U}_4^{c*} \tilde{U}_4^c - m_{\tilde{D}_4}^2 \tilde{D}_4^{c*} \tilde{D}_4^c \\
&\quad - m_{\tilde{Q}_5}^2 \tilde{Q}_5^{c\dagger} \tilde{Q}_5^c - m_{\tilde{U}_5}^2 \tilde{U}_5^* \tilde{U}_5 - m_{\tilde{D}_5}^2 \tilde{D}_5^* \tilde{D}_5 - m_{\tilde{L}_4}^2 \tilde{L}_4^\dagger \tilde{L}_4 - m_{\tilde{\nu}_4}^2 \tilde{N}_4^{c*} \tilde{N}_4^c \\
&\quad - m_{\tilde{e}_4}^2 \tilde{E}_4^{c*} \tilde{E}_4^c - m_{\tilde{L}_5}^2 \tilde{L}_5^{c\dagger} \tilde{L}_5^c - m_{\tilde{\nu}_5}^2 \tilde{N}_5^* \tilde{N}_5 - m_{\tilde{e}_5}^2 \tilde{E}_5^* \tilde{E}_5 - m_{\Phi_B}^2 \Phi_B^* \Phi_B \\
&\quad - m_{\varphi_B}^2 \varphi_B^* \varphi_B - m_{\Phi_L}^2 \Phi_L^* \Phi_L - m_{\varphi_L}^2 \varphi_L^* \varphi_L - \left(m_B \lambda_B \lambda_B + m_L \lambda_L \lambda_L + h.c. \right) \\
&\quad + \left\{ A_{u_4} Y_{u_4} \tilde{Q}_4 H_u \tilde{U}_4^c + A_{d_4} Y_{d_4} \tilde{Q}_4 H_d \tilde{D}_4^c + A_{u_5} Y_{u_5} \tilde{Q}_5 H_u \tilde{U}_5^c + A_{d_5} Y_{d_5} \tilde{Q}_5 H_u \tilde{D}_5^c \right. \\
&\quad \left. + A_{BQ} \lambda_Q \tilde{Q}_4 \tilde{Q}_5^c \Phi_B + A_{BU} \lambda_U \tilde{U}_4^c \tilde{U}_5^c \varphi_B + A_{BD} \lambda_D \tilde{D}_4^c \tilde{D}_5^c \varphi_B + B_B \mu_B \Phi_B \varphi_B + h.c. \right\} \\
&\quad + \left\{ A_{e_4} Y_{e_4} \tilde{L}_4 H_d \tilde{E}_4^c + A_{\nu_4} Y_{\nu_4} \tilde{L}_4 H_u \tilde{N}_4^c + A_{e_5} Y_{e_5} \tilde{L}_5 H_u \tilde{E}_5^c + A_{\nu_5} Y_{\nu_5} \tilde{L}_5 H_d \tilde{N}_5^c \right. \\
&\quad \left. + A_N Y_\nu \tilde{L} H_u \tilde{N}^c + A_{N^c} \lambda_{N^c} \tilde{N}^c \tilde{N}^c \varphi_L + B_L \mu_L \Phi_L \varphi_L + h.c. \right\} \\
&\quad + \left\{ A_1 \lambda_1 \tilde{Q} \tilde{Q}_5^c X + A_2 \lambda_2 \tilde{U}^c \tilde{U}_5^c X' + A_3 \lambda_3 \tilde{D}^c \tilde{D}_5^c X' + B_X \mu_X X X' + h.c. \right\}.
\end{aligned} \tag{6}$$

The used mass matrices can be found in the works [49, 58]. The relevant Feynman rules same as those in MSSM for the present computation are collected in Ref. [58]. The Feynman rules for vertices uniquely used in the BLMSM are as follows:

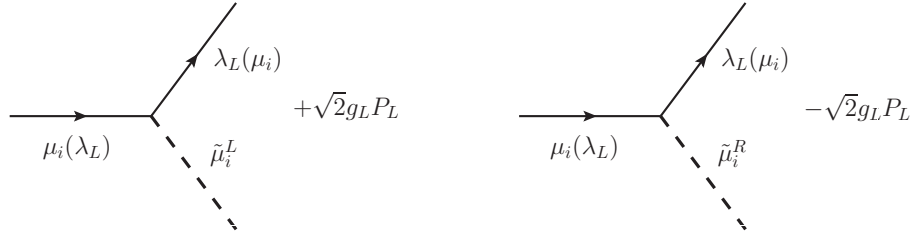


FIG. 1: Feynman rules for the unique vertices in the BLMSM.

III. FORMULATION

A. The muon MDM

The lepton MDM can be obtained from the following effective Lagrangian by using the on-shell condition for the external leptons,

$$\mathcal{L}_{MDM} = \frac{e}{4m_l} a_l \bar{l} \sigma^{\mu\nu} l F_{\mu\nu}, \quad (7)$$

with $\sigma^{\mu\nu} = i[\gamma_\mu, \gamma_\nu]/2$. e and l denote the electric charge and the lepton fermion, respectively. $F_{\mu\nu}$ is the electromagnetic field strength, and m_l is the lepton mass.

The Feynman amplitude can be expressed by these dimension 6 operators [59] with the effective Lagrangian method for the process $l^I \rightarrow l^I + \gamma$. The dimension 8 operators are suppressed by additional factor $\frac{m_l^2}{M_{SUSY}^2} \sim (10^{-7}, 10^{-8})$, which are neglected safely. Therefore, these dimension 6 operators are enough to use in future calculations. The operators related to lepton MDM are $\mathcal{O}_{2,3,6}^{L,R}$. The lepton MDM is the combination of the Wilson coefficients $C_{2,3,6}^{L,R}$. Here, $\mathcal{D}_\mu = \partial_\mu + ieA_\mu$ and $P_{L,R} = \frac{1 \mp \gamma_5}{2}$. The specific forms of those dimension 6 operators are

$$\begin{aligned} \mathcal{O}_1^{L,R} &= \frac{1}{(4\pi)^2} \bar{l} (i\mathcal{D})^3 P_{L,R} l, & \mathcal{O}_2^{L,R} &= \frac{eQ_f}{(4\pi)^2} \overline{(i\mathcal{D}_\mu l)} \gamma^\mu F \cdot \sigma P_{L,R} l, \\ \mathcal{O}_3^{L,R} &= \frac{eQ_f}{(4\pi)^2} \bar{l} F \cdot \sigma \gamma^\mu P_{L,R} (i\mathcal{D}_\mu l), & \mathcal{O}_4^{L,R} &= \frac{eQ_f}{(4\pi)^2} \bar{l} (\partial^\mu F_{\mu\nu}) \gamma^\nu P_{L,R} l, \\ \mathcal{O}_5^{L,R} &= \frac{m_l}{(4\pi)^2} \bar{l} (i\mathcal{D})^2 P_{L,R} l, & \mathcal{O}_6^{L,R} &= \frac{eQ_f m_l}{(4\pi)^2} \bar{l} F \cdot \sigma P_{L,R} l. \end{aligned} \quad (8)$$

1. The mass eigenstate

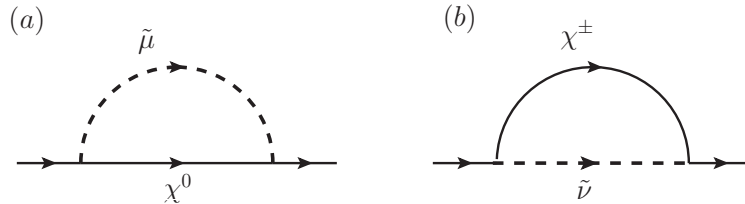


FIG. 2: The two one-loop diagrams drawn in the mass eigenstate for $l^I \rightarrow l^I + \gamma$. The external photon line has to be attached to the charged internal lines.

The analytical forms of one-loop corrections in BLMSSM are similar to that of MSSM. The differences are: 1. the squared mass matrixes of scalar leptons because of new parameters g_L, \bar{v}_L, v_L and so on; 2. three-generation right-handed neutrinos are introduced, which lead to the neutrinos and scalar neutrinos are doubled. In the BLMSSM, there are four parts contributing to muon MDM: 1. scalar muon ($\tilde{\mu}$) and neutralino (χ^0) [Fig. 2(a)]; 2. scalar neutrino ($\tilde{\nu}$) and chargino (χ^\pm) [Fig. 2(b)]; 3. neutral Higgs (H^0) and muon (μ); 4. charged Higgs (H^\pm) and neutrino (ν).

The one-loop Higgs contribution to muon MDM is very small, because it is inhibited by the factor $\frac{m_\mu^2}{m_W^2}$. The mass matrix of neutrinos and the squared mass matrix of scalar neutrinos are extended to 6×6 . From these analysis, the contributions of type 3 and 4 are entirely negligible. Due to the mass of the new vector boson Z_L being greater than 5.1 TeV, the one-loop contributions from Z_L -muon are suppressed by the factor $\frac{m_Z^2}{m_{Z_L}^2} \sim 4 \times 10^{-4}$. So, we neglect Z_L -muon one-loop contributions.

Therefore, the one-loop new physics contributions to muon MDM are given entirely by the Fig. 2. On the basis of the one-loop self-energy diagrams, we can get the one-loop triangle diagrams by attaching a photon on the internal line in all possible ways. These diagrams have been comprehensively discussed in the BLMSSM with the mass eigenstate [36], and the exact results have been derived. We show the general results in the form:

$$a_\mu^{BL} = a_\mu^{\tilde{\mu}\chi^0} + a_\mu^{\tilde{\nu}\chi^\pm}, \quad (9)$$

with

$$a_\mu^{\tilde{\mu}\chi^0} = -\frac{e^2}{2s_W^2} \sum_{i=1}^6 \sum_{j=1}^4 \left[\text{Re}[(\mathcal{S}_1)_{ij}^I (\mathcal{S}_2)_{ij}^{I*}] \sqrt{x_{\chi_j^0} x_{\tilde{L}_i}} x_{\tilde{L}_i} \frac{\partial^2 \mathcal{B}(x_{\chi_j^0}, x_{\tilde{L}_i})}{\partial x_{\tilde{L}_i}^2} \right. \\ \left. + \frac{1}{3} (|(\mathcal{S}_1)_{ij}^I|^2 + |(\mathcal{S}_2)_{ij}^I|^2) x_{\tilde{L}_i} x_{\tilde{L}_i} \frac{\partial \mathcal{B}_1(x_{\chi_j^0}, x_{\tilde{L}_i})}{\partial x_{\tilde{L}_i}} \right], \quad (10)$$

$$a_\mu^{\tilde{\nu}\chi^\pm} = \frac{e^2}{s_W^2} \sum_{J=1}^3 \sum_{i,j=1}^2 \left[\sqrt{2} \frac{m_{l^I}}{m_W} \text{Re}[Z_+^{1j} Z_-^{2j}] |Z_{\tilde{\nu}^I J}^{1i}|^2 \sqrt{x_{\chi_j^\pm} x_{l^I}} \mathcal{B}_1(x_{\tilde{\nu}^I J}, x_{\chi_j^\pm}) \right. \\ \left. + \frac{1}{3} (|Z_+^{1j} Z_{\tilde{\nu}^I J}^{1i*}|^2 + \frac{m_{l^I}^2}{2m_W^2} |Z_-^{2j*} Z_{\tilde{\nu}^I J}^{1i*}|^2) x_{\chi_j^\pm} x_{l^I} \frac{\partial \mathcal{B}_1(x_{\tilde{\nu}^I J}, x_{\chi_j^\pm})}{\partial x_{\chi_j^\pm}} \right]. \quad (11)$$

Here, $x_i = \frac{m_i^2}{M_{SUSY}^2}$, m_i is the particle mass. The abbreviation notations $s_W = \sin \theta_W$, $c_W = \cos \theta_W$, where θ_W is the Weinberg angle. We define the functions $\mathcal{B}(x, y)$, $\mathcal{B}_1(x, y)$

$$\mathcal{B}(x, y) = \frac{1}{16\pi^2} \left(\frac{x \ln x}{y - x} + \frac{y \ln y}{x - y} \right), \quad \mathcal{B}_1(x, y) = \left(\frac{\partial}{\partial y} + \frac{y}{2} \frac{\partial^2}{\partial y^2} \right) \mathcal{B}(x, y). \quad (12)$$

The couplings $(\mathcal{S}_1)_{ij}^I$, $(\mathcal{S}_2)_{ij}^I$ are shown as

$$\begin{aligned} (\mathcal{S}_1)_{ij}^I &= \frac{1}{c_W} Z_{\tilde{L}}^{Ii*} (Z_N^{1j} s_W + Z_N^{2j} c_W) - \frac{m_{l^I}}{\cos \beta m_W} Z_{\tilde{L}}^{(I+3)i*} Z_N^{3j}, \\ (\mathcal{S}_2)_{ij}^I &= -2 \frac{s_W}{c_W} Z_{\tilde{L}}^{(I+3)i*} Z_N^{1j*} - \frac{m_{l^I}}{\cos \beta m_W} Z_{\tilde{L}}^{Ii*} Z_N^{3j*}. \end{aligned} \quad (13)$$

The matrices $Z_{\tilde{L}}$, Z_N diagonalize the mass matrices of scalar lepton and neutralino, respectively. Z_- , Z_+ are used to diagonalize the chargino mass matrix. The mass squared matrix of scalar neutrino are diagonalized by $Z_{\tilde{\nu}^{IJ}}$.

2. The mass insertion approximation

Through the above discussion of BLMSSM contributions to muon MDM, we can know that the contributions do not represent an enhancement proportional to $\frac{m_\chi}{m_{l^I}}$, because it is suppressed by the combined rotation matrixes. In fact, they produce an overall enhancement factor $\tan \beta$ [60, 61]. In other words, $|a_\mu^{BL}|$ becomes large as $\tan \beta$ increases. Thus, it's more convenient to use the mass insertion approximation (MIA) [58, 60, 62, 63] to calculate, and the role of parameters can be more clearly displayed. However, the mass eigenstate in the previous section is more appropriate for an exact evaluation. Now, we obtain the specific forms of the one-loop contributions by using MIA in the BLMSSM.

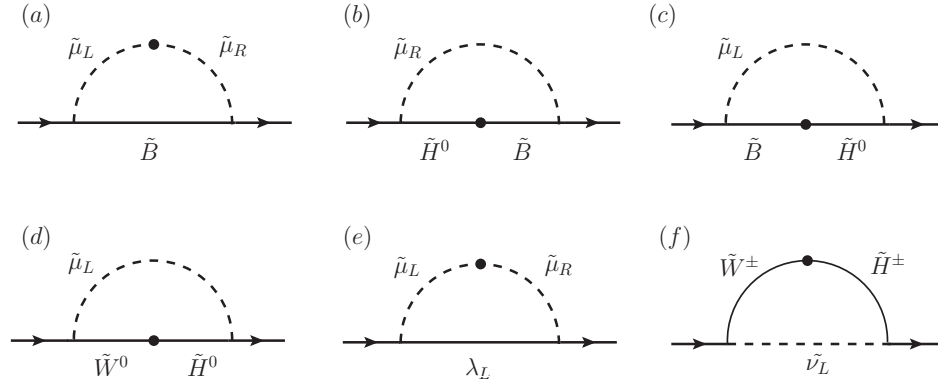


FIG. 3: Feynman diagrams for generating muon MDM and lepton EDM based on MIA. The external photons are connected to the charged internal lines in all possible ways.

a. The one-loop contributions from \tilde{B} - $\tilde{\mu}_L$ - $\tilde{\mu}_R$.

$$\begin{aligned} a_\mu^{BL,(a)} &= 2g_1^2 x_\mu \sqrt{x_1 x_{\mu_H}} \tan \beta [I_1(x_1, x_{\tilde{\mu}_L}, x_{\tilde{\mu}_R}) + I_2(x_1, x_{\tilde{\mu}_L}, x_{\tilde{\mu}_R}) \\ &\quad - J_1(x_1, x_{\tilde{\mu}_L}, x_{\tilde{\mu}_R}) - J_2(x_1, x_{\tilde{\mu}_L}, x_{\tilde{\mu}_R}) - J_3(x_1, x_{\tilde{\mu}_L}, x_{\tilde{\mu}_R})]. \end{aligned} \quad (14)$$

with $m_1 = m_{\tilde{B}}$. The functions $I_1(x, y, z)$, $I_2(x, y, z)$, $J_1(x, y, z)$, $J_2(x, y, z)$ and $J_3(x, y, z)$ are defined as

$$I_1(x, y, z) = \frac{1}{16\pi^2} \left\{ \frac{(z^2 - xy) \log z}{(x - z)^2(y - z)^2} - \frac{1}{(x - z)(y - z)} - \frac{x \log x}{(x - y)(x - z)^2} + \frac{y \log y}{(x - y)(y - z)^2} \right\}, \quad (15)$$

$$I_2(x, y, z) = \frac{1}{16\pi^2} \left\{ \frac{1}{(x - y)(y - z)} - \frac{x \log x}{(x - y)^2(x - z)} + \frac{(y^2 - xz) \log y}{(x - y)^2(y - z)^2} + \frac{z \log z}{(x - z)(y - z)^2} \right\}, \quad (16)$$

$$J_1(x, y, z) = \frac{1}{32\pi^2} \left\{ \frac{x(z - 3y) + z(y + z)}{(x - z)^2(y - z)^2} - \frac{2x^2 \log x}{(x - y)(x - z)^3} + \frac{2y^2 \log y}{(x - y)(y - z)^3} - \frac{2[x^2y^2 + z^3(x + y) - 3xyz^2] \log z}{(x - z)^3(y - z)^3} \right\}, \quad (17)$$

$$J_2(x, y, z) = \frac{1}{32\pi^2} \left\{ \frac{x(y - 3z) + y(y + z)}{(x - y)^2(y - z)^2} - \frac{2x^2 \log x}{(x - y)^3(x - z)} + \frac{2[x^2z^2 + xy^2(y - 3z) + y^3z] \log y}{(x - y)^3(y - z)^3} + \frac{2z^2 \log z}{(x - z)(z - y)^3} \right\}, \quad (18)$$

$$J_3(x, y, z) = \frac{1}{16\pi^2} \left\{ \frac{x(y + z) - 2yz}{(x - y)(x - z)(y - z)^2} - \frac{x^2 \log x}{(x - y)^2(x - z)^2} + \frac{y[y(y + z) - 2xz] \log y}{(x - y)^2(y - z)^3} + \frac{z[z(y + z) - 2xy] \log z}{(x - z)^2(z - y)^3} \right\}. \quad (19)$$

b. The one-loop contributions from \tilde{B} - \tilde{H}^0 - $\tilde{\mu}_R$.

$$a_\mu^{BL,(b)} = -2g_1^2 x_\mu \sqrt{x_1 x_{\mu_H}} \tan \beta [I_1(x_1, x_{\mu_H}, x_{\tilde{\mu}_R}) - J_1(x_1, x_{\mu_H}, x_{\tilde{\mu}_R})]. \quad (20)$$

c. The one-loop contributions from \tilde{B} - \tilde{H}^0 - $\tilde{\mu}_L$.

$$a_\mu^{BL,(c)} = g_1^2 x_\mu \sqrt{x_1 x_{\mu_H}} \tan \beta [I_1(x_1, x_{\mu_H}, x_{\tilde{\mu}_L}) - J_1(x_1, x_{\mu_H}, x_{\tilde{\mu}_L})]. \quad (21)$$

d. The one-loop contributions from \tilde{W}^0 - \tilde{H}^0 - $\tilde{\mu}_L$.

$$a_\mu^{BL,(d)} = -g_2^2 x_\mu \sqrt{x_2 x_{\mu_H}} \tan \beta [I_1(x_2, x_{\mu_H}, x_{\tilde{\mu}_L}) - J_1(x_2, x_{\mu_H}, x_{\tilde{\mu}_L})]. \quad (22)$$

here, $m_2 = m_{\tilde{W}^0} = m_{\tilde{W}^\pm}$.

e. The one-loop contributions from λ_L - $\tilde{\mu}_L$ - $\tilde{\mu}_R$.

$$a_\mu^{BL,(e)} = -4g_L^2 x_\mu \sqrt{x_L x_{\mu_H}} \tan \beta [I_1(x_L, x_{\tilde{\mu}_L}, x_{\tilde{\mu}_R}) + I_2(x_L, x_{\tilde{\mu}_L}, x_{\tilde{\mu}_R}) - J_1(x_L, x_{\tilde{\mu}_L}, x_{\tilde{\mu}_R}) - J_2(x_L, x_{\tilde{\mu}_L}, x_{\tilde{\mu}_R}) - J_3(x_L, x_{\tilde{\mu}_L}, x_{\tilde{\mu}_R})]. \quad (23)$$

f. The one-loop contributions from \tilde{W}^\pm - \tilde{H}^\pm - $\tilde{\nu}_L$.

$$a_\mu^{BL,(f)} = 2g_2^2 x_\mu \sqrt{x_2 x_{\mu_H}} \tan \beta [J_2(x_2, x_{\mu_H}, x_{\tilde{\nu}_L}) + J_4(x_2, x_{\mu_H}, x_{\tilde{\nu}_L}) + J_5(x_2, x_{\mu_H}, x_{\tilde{\nu}_L})]. \quad (24)$$

We define the functions $J_4(x, y, z)$ and $J_5(x, y, z)$ as

$$J_4(x, y, z) = \frac{1}{16\pi^2} \left\{ \frac{z(x+y) - 2xy}{(x-y)^2(x-z)(y-z)} + \frac{x[x(x+y) - 2yz] \log x}{(x-y)^3(x-z)^2} \right. \\ \left. + \frac{y[y(x+y) - 2xz] \log y}{(y-x)^3(y-z)^2} - \frac{z^2 \log z}{(x-z)^2(y-z)^2} \right\}, \quad (25)$$

$$J_5(x, y, z) = \frac{1}{32\pi^2} \left\{ \frac{x^2 + x(y+z) - 3yz}{(x-y)^2(x-z)^2} - \frac{2[x^3(y+z) - 3x^2yz + y^2z^2] \log x}{(x-y)^3(x-z)^3} \right. \\ \left. + \frac{2y^2 \log y}{(x-y)^3(y-z)} + \frac{2z^2 \log z}{(x-z)^3(z-y)} \right\}. \quad (26)$$

The one-loop contributions to muon MDM can be expressed as

$$a_\mu^{\tilde{\mu}\chi^0} \simeq a_\mu^{BL,(a)} + a_\mu^{BL,(b)} + a_\mu^{BL,(c)} + a_\mu^{BL,(d)} + a_\mu^{BL,(e)}, \\ a_\mu^{\tilde{\nu}\chi^\pm} \simeq a_\mu^{BL,(f)}. \quad (27)$$

We ought to notice that the contributions to muon MDM are related to $\tan \beta$ and x_i in the Eqs. (14), (20)–(24). This situation is consistent with MSSM. The contribution related to the new gaugino λ_L is shown in Eq. (23), which includes the new gauge coupling constant g_L . Furthermore, we obtain the conclusion that $a_\mu^{BL,(a)}$, $a_\mu^{BL,(e)}$ and $a_\mu^{BL,(f)}$ occupy the dominant position after numerical comparison. When m_{λ_L} is negative, the signs of $a_\mu^{BL,(a)}$, $a_\mu^{BL,(e)}$ and $a_\mu^{BL,(f)}$ are the same. We can get the reasonable corrections of new physics.

3. Degenerate result

Next, we assume that all the masses of the superparticles are almost degenerate to more clearly know the influential factor on a_μ^{BL} . The masses of superparticles ($m_1, m_2, \mu_H, m_{\tilde{\nu}_L}, m_{\tilde{\mu}_R}, m_{\tilde{\mu}_L}, m_L$) are equal to M_{SUSY} [40]:

$$|m_1| = |m_2| = |\mu_H| = m_{\tilde{\nu}_L} = m_{\tilde{\mu}_R} = m_{\tilde{\mu}_L} = |m_L| = M_{SUSY}. \quad (28)$$

The functions can be simplified as

$$I_1(1, 1, 1) = I_2(1, 1, 1) = \frac{1}{96\pi^2}, \\ J_1(1, 1, 1) = J_2(1, 1, 1) = J_3(1, 1, 1) = J_4(1, 1, 1) = J_5(1, 1, 1) = \frac{1}{192\pi^2}. \quad (29)$$

The one-loop MSSM results (chargino-sneutrino, neutralino-smuon) in this case are consistent with the results of Ref. [60]. Here, $\text{sign}[m_1] = \text{sign}[m_2] = \text{sign}[\mu_H] = 1$.

$$a_\mu^{MSSM} \simeq \frac{1}{192\pi^2} \frac{m_\mu^2}{M_{SUSY}^2} (g_1^2 + 5g_2^2) \tan \beta. \quad (30)$$

In the BLSSM, the one-loop results of muon MDM are given by

$$\begin{aligned} a_\mu^{BL} \simeq & \frac{1}{192\pi^2} \frac{m_\mu^2}{M_{SUSY}^2} (g_1^2 + 5g_2^2) \tan \beta \\ & - \frac{1}{48\pi^2} \frac{m_\mu^2}{M_{SUSY}^2} g_L^2 \tan \beta \text{sign}[\mu_H m_L]. \end{aligned} \quad (31)$$

The corrections can reach large value, when $\text{sign}[m_1] = \text{sign}[m_2] = \text{sign}[\mu_H] = 1$ and $\text{sign}[m_L] = -1$.

$$a_\mu^{BL} \rightarrow \frac{1}{192\pi^2} \frac{m_\mu^2}{M_{SUSY}^2} (g_1^2 + 5g_2^2 + 4g_L^2) \tan \beta. \quad (32)$$

According to the above expressions, we study the effect of M_{SUSY} , $\tan \beta$ and g_L on the BLSSM contributions to muon MDM. The results are shown in Fig. 4. First, we plot the results for $\tan \beta = 50$ in the g_L - M_{SUSY} plane. As we can see, if we take a smaller value of M_{SUSY} , the a_μ^{BL} is enhanced in the large g_L region. Next, the upper right figure denotes $\tan \beta$ - M_{SUSY} plane when $g_L = 0.45$. The results imply that large $\tan \beta$ and small M_{SUSY} can produce suitable BLSSM corrections to compensate the departure. At last, the bottom figure shows the results in the plane of $\tan \beta$ versus g_L . When the values of $\tan \beta$ and g_L enlarge, the value of a_μ^{BL} also increases, but $\tan \beta$ is more sensitive than g_L . It shows that M_{SUSY} , $\tan \beta$ and g_L are sensitive, and have a direct effect on a_μ^{BL} .

B. The lepton EDM

The lepton EDM can be obtained by using effective Lagrange method, and the Feynman amplitudes can be expressed by these dimension 6 operators in Eq. (8). Adopting on-shell condition for external leptons, only $\mathcal{O}_{2,3,6}^\mp$ contribute to lepton EDM. This is consistent with muon MDM. The lepton EDM is expressed as

$$\mathcal{L}_{EDM} = -\frac{i}{2} d_l \bar{l} \sigma^{\mu\nu} \gamma_5 l F_{\mu\nu}. \quad (33)$$

In the BLSSM, there are essentially two types of one-loop triangle diagrams which contribute to d_l^{BL} : 1. the neutralino-slepton diagram; 2. the chargino-sneutrino diagram.

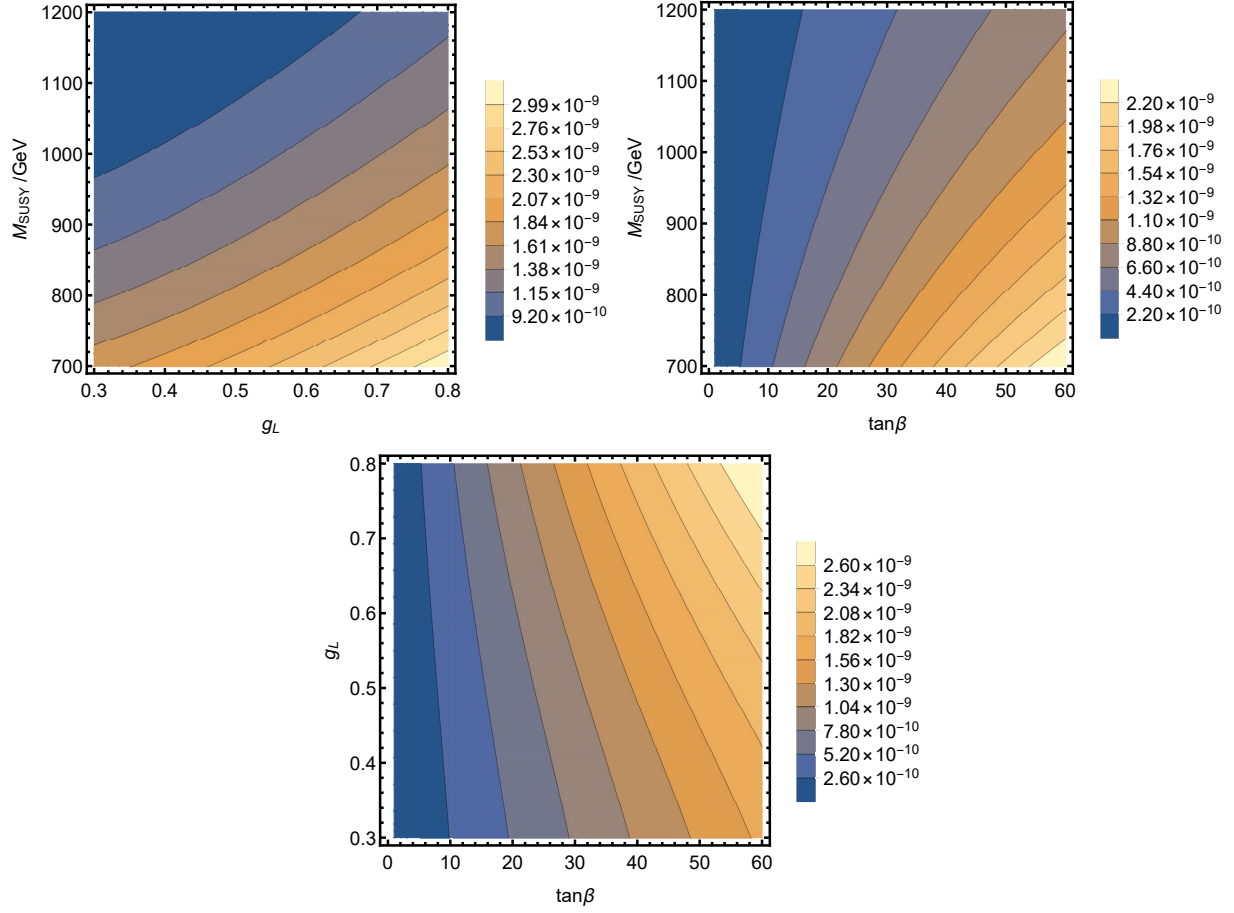


FIG. 4: The effects of M_{SUSY} , $\tan\beta$ and g_L on a_μ^{BL} . The upper left figure denotes g_L - M_{SUSY} plane with $\tan\beta = 50$. The upper right figure denotes $\tan\beta$ - M_{SUSY} plane with $g_L = 0.45$. The bottom figure denotes $\tan\beta$ - g_L plane with $M_{SUSY} = 1000$ GeV.

Using the MIA, we can obtain six diagrams that have major contributions to d_l^{BL} , which are shown in Fig. 3. These contributions can be given by

$$\begin{aligned}
d_l^{BL,(a)} &= \frac{eg_1^2}{M_{SUSY}} \sqrt{x_l x_1 x_{\mu_H}} e^{i*\theta_1} e^{i*\theta_{\mu_H}} \tan\beta [I_1(x_1, x_{\tilde{L}_L}, x_{\tilde{L}_R}) + I_2(x_1, x_{\tilde{L}_L}, x_{\tilde{L}_R}) \\
&\quad - J_1(x_1, x_{\tilde{L}_L}, x_{\tilde{L}_R}) - J_2(x_1, x_{\tilde{L}_L}, x_{\tilde{L}_R}) - J_3(x_1, x_{\tilde{L}_L}, x_{\tilde{L}_R})], \\
d_l^{BL,(b)} &= \frac{eg_1^2}{M_{SUSY}} \sqrt{x_l x_1 x_{\mu_H}} e^{i*\theta_1} e^{i*\theta_{\mu_H}} \tan\beta [I_1(x_1, x_{\mu_H}, x_{\tilde{L}_R}) - J_1(x_1, x_{\mu_H}, x_{\tilde{L}_R})], \\
d_l^{BL,(c)} &= -\frac{eg_1^2}{2M_{SUSY}} \sqrt{x_l x_1 x_{\mu_H}} e^{i*\theta_1} e^{i*\theta_{\mu_H}} \tan\beta [I_1(x_1, x_{\mu_H}, x_{\tilde{L}_L}) - J_1(x_1, x_{\mu_H}, x_{\tilde{L}_L})], \\
d_l^{BL,(d)} &= \frac{eg_2^2}{2M_{SUSY}} \sqrt{x_l x_2 x_{\mu_H}} e^{i*\theta_2} e^{i*\theta_{\mu_H}} \tan\beta [I_1(x_2, x_{\mu_H}, x_{\tilde{L}_L}) - J_1(x_2, x_{\mu_H}, x_{\tilde{L}_L})], \\
d_l^{BL,(e)} &= -\frac{2eg_L^2}{M_{SUSY}} \sqrt{x_l x_L x_{\mu_L}} e^{i*\theta_L} e^{i*\theta_{\mu_L}} \tan\beta [I_1(x_L, x_{\tilde{L}_L}, x_{\tilde{L}_R}) + I_2(x_L, x_{\tilde{L}_L}, x_{\tilde{L}_R})]
\end{aligned}$$

$$\begin{aligned}
& -J_1(x_L, x_{\tilde{L}_L}, x_{\tilde{L}_R}) - J_2(x_L, x_{\tilde{L}_L}, x_{\tilde{L}_R}) - J_3(x_L, x_{\tilde{L}_L}, x_{\tilde{L}_R})], \\
d_l^{BL,(f)} = & -\frac{eg_2^2}{M_{SUSY}} \sqrt{x_l x_2 x_{\mu_H}} e^{i*\theta_2} e^{i*\theta_{\mu_H}} \tan \beta [J_2(x_2, x_{\mu_H}, x_{\tilde{\nu}_L}) + J_4(x_2, x_{\mu_H}, x_{\tilde{\nu}_L}) \\
& + J_5(x_2, x_{\mu_H}, x_{\tilde{\nu}_L})].
\end{aligned} \tag{34}$$

The one-loop contributions to lepton EDM can be expressed as

$$\begin{aligned}
d_l^{BL} &= d_l^{\tilde{l}\chi^0} + d_l^{\tilde{\nu}\chi^\pm}, \\
d_l^{\tilde{l}\chi^0} &\simeq d_l^{BL,(a)} + d_l^{BL,(b)} + d_l^{BL,(c)} + d_l^{BL,(d)} + d_l^{BL,(e)}, \\
d_l^{\tilde{\nu}\chi^\pm} &\simeq d_l^{BL,(f)}.
\end{aligned} \tag{35}$$

In Eq. (34), some parameters are defined as follows

$$\begin{aligned}
m_{\tilde{B}} &= M_1 * e^{i*\theta_1}, \quad m_{\tilde{W}^0} = m_{\tilde{W}^\pm} = M_2 * e^{i*\theta_2}, \quad \mu_H = M_{\mu_H} * e^{i*\theta_{\mu_H}}, \\
\mu_L &= M_{\mu_L} * e^{i*\theta_{\mu_L}}, \quad m_L = M_L * e^{i*\theta_L}, \quad x_l = \frac{m_l^2}{M_{SUSY}^2}, \quad x_{\tilde{\nu}_L} = \frac{m_{\tilde{\nu}_L}^2}{M_{SUSY}^2}, \\
x_{\tilde{L}_L} &= \frac{m_{\tilde{L}_L}^2}{M_{SUSY}^2}, \quad x_{\tilde{L}_R} = \frac{m_{\tilde{L}_R}^2}{M_{SUSY}^2}, \quad x_i = \frac{|M_i|^2}{M_{SUSY}^2}.
\end{aligned} \tag{36}$$

M_i means the above five particle masses in the form of complex function ($M_1, M_2, M_{\mu_H}, M_{\mu_L}, M_L$). θ_1, θ_2 and θ_{μ_H} are the CP violating phases of the parameters $m_{\tilde{B}}, m_{\tilde{W}^0}$ ($m_{\tilde{W}^\pm}$), and μ_H . θ_{μ_L} and θ_L are the CP violating phases of new parameters μ_L and m_L . In these formulas, the CP violating phases are conspicuous, and we can more easily observe the cancellation between the CP violating phases.

IV. NUMERICAL RESULTS

In this section, we first discuss the numerical difference between the mass eigenstate and the mass insertion approximation. Then, the one-loop contributions of the muon MDM and lepton (e, μ, τ) EDM are discussed numerically via the MIA. In the numerical discussion, we consider the latest experimental limitations of particles [63–67]. The lightest CP-even Higgs mass $m_{h^0} = 125.1$ GeV [68, 69]. The slepton mass is greater than 700 GeV, and the chargino mass is greater than 1100 GeV [62]. Taking Z_L boson mass is greater than 5.1 TeV to satisfy the mass constraint from LHC experiments [70].

A. The relative error between the two methods

In order to determine the accuracy of the MIA expressions, we discuss the numerical difference between the mass eigenstate expressions and the MIA expressions from the point value and one-dimensional graph. Firstly, we discuss the point value. We set the same parameters of the two expressions to the same values, i.e., $\tan \beta = 50$, $m_1 = 300$ GeV, $m_2 = 1100$ GeV and $g_L = 1/3$, and adjust the other parameters to make the masses of particles in the two methods meet the mass limits while maintaining roughly equal. The a_μ^{BL} obtained by the mass eigenstate expressions and the MIA expressions are 2.279×10^{-9} and 2.257×10^{-9} , respectively. The relative error ($\frac{2.279 \times 10^{-9} - 2.257 \times 10^{-9}}{2.279 \times 10^{-9}}$) is about 0.96%, which is relatively small.

The comparisons of the results of the two expressions are shown in Fig. 5. The experimental limitations are denoted by the colored areas, where light green area represents 1σ , light orange area represents 2σ . The lines of these three figures are within the colored areas, which can well satisfy the experimental constraint. In Fig. 5(a), the two lines have similar behavior, that is, slowly increase and then slowly decrease. The two lines are relatively close, and there are two intersections. In Fig. 5(b), the two lines almost coincide in the area m_2 (1000, 1500) GeV and are very close in the remaining area. In Fig. 5(c), the two lines have an upward trend and almost coincide in the area g_L (0.3, 0.35). Therefore, according to these diagrams, we can obtain that the results of the two expressions are very similar, and the accuracy of the MIA results is verified.

B. The muon MDM by MIA

In this subsection, we numerically calculate the BLMSSM contributions to muon MDM (a_μ^{BL}). Based on the above analysis of the mass insertion approximation, a_μ^{BL} mainly depends on 9 parameters, i.e., $\tan \beta$, g_L , m_1 , m_2 , m_L , μ_H , $m_{\tilde{\nu}_L}$, $m_{\tilde{\mu}_R}$, $m_{\tilde{\mu}_L}$. We take these parameters as free parameters and compute the BLMSSM contributions to the muon MDM for a given set of parameters, with the parameter $M_{SUSY} = 1000$ GeV.

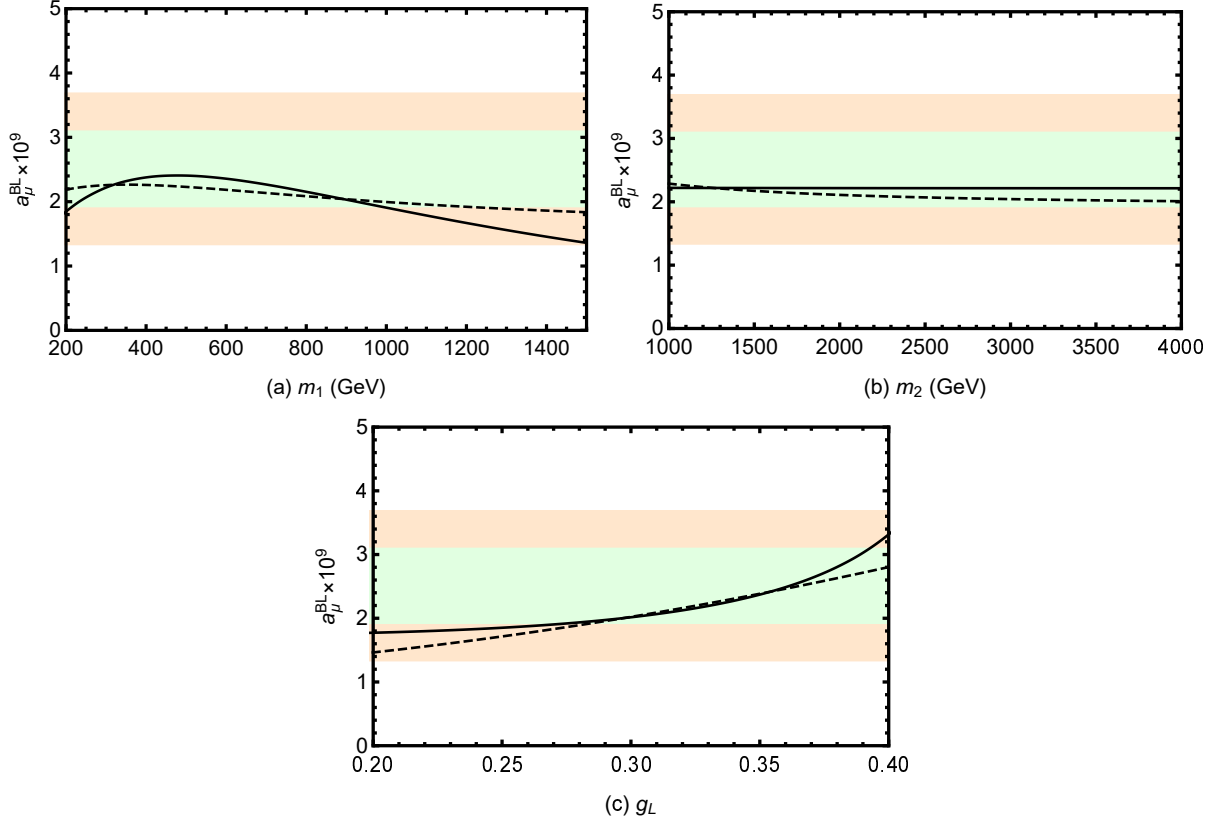


FIG. 5: The BLMSM contributions to muon MDM (a_μ^{BL}) versus m_1 (a), m_2 (b) and g_L (c) are plotted by solid line (the mass eigenstate expressions) and dashed line (the mass insertion approximation expressions).

1. One-dimensional graphs

In this part, we take $m_1 = 300$ GeV, $m_L = -300$ GeV, $m_{\tilde{\nu}_L} = 150$ GeV, $m_{\tilde{\mu}_L} = 700$ GeV, $m_{\tilde{\mu}_R} = 700$ GeV, and plot the following a_μ^{BL} schematic diagram affected by different parameters. The colored areas show the experimental limitations, with light green area for 1σ and light orange area for 2σ .

In Fig. 6, we plot the results versus g_L with $m_2 = 1100$ GeV and $\mu_H = 1100$ GeV. Beyond MSSM, there is a parameter g_L that corresponds to the coupling constant of the $U(1)_L$ gauge. From the analysis by MIA, g_L is an important parameter that appears in Eq. (23). It can be seen that from bottom to top are solid line ($\tan\beta = 30$), dashed line ($\tan\beta = 40$) and dotted line ($\tan\beta = 50$), and the overall trend of the three lines is upward. This conclusion can be seen more intuitively from Eq. (32). The dotted line is entirely in

the colored areas, the dashed line part of $0.22 - 0.6$ is in the colored areas, the solid line part of $0.4 - 0.6$ is in the colored areas. That is to say, $\tan\beta$ is a sensitive parameter and larger $\tan\beta$ leads to larger a_μ^{BL} . The value of a_μ^{BL} is around 2.5×10^{-9} , and it can better meet the experimental limitations.

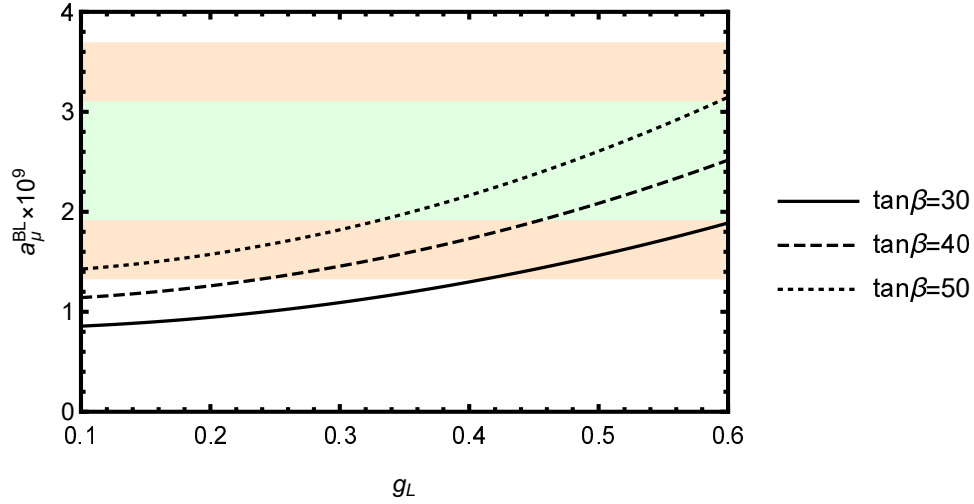


FIG. 6: The BLMSSM contributions to muon MDM (a_μ^{BL}) versus g_L .

Similarly, we take $m_2 = 1100$ GeV and $\mu_H = 1100$ GeV, and plot the BLMSSM contributions to muon MDM varying with $\tan\beta$ in Fig. 7. The parameter $\tan\beta$ is ratio of the VEVs of the two Higgs doublets ($\tan\beta = v_u/v_d$). $\tan\beta$ is contained in each one-loop contribution and is proportional relationship. The solid (dashed, dotted) line corresponds to the results with $g_L = 0.25$ (0.45 , 0.65). We find that $\tan\beta$ and a_μ^{BL} are positively correlated, which is the same effect reflected by Eqs. (14), (20)–(24). The colored areas contain more parts of the dotted line. The characteristic obtained here is consistent with those obtained in Fig. 6. Large g_L and $\tan\beta$ can lead to large BLMSSM contributions. Thus, the contributions can be influenced obviously by the parameters g_L and $\tan\beta$. The value of a_μ^{BL} is around 2.5×10^{-9} , which can well compensate for the deviation.

For better numerical results, we set $\tan\beta = 50$ and $\mu_H = 1100$ GeV. The solid line ($g_L = 0.25$), dashed line ($g_L = 0.45$) and dotted line ($g_L = 0.55$) varying with m_2 are shown in Fig. 8. m_2 expresses the particle mass of \tilde{W}^0 (\tilde{W}^\pm), which directly affects the one-loop contributions from Figs. 3(d), 3(f). The three lines are all decreasing functions, when m_2 turns large from 1100 GeV to 3000 GeV. The downward trend slowly becomes weak. The reason is that the contributions are proportional to $\sqrt{x_2} = \frac{m_2}{M_{SUSY}}$, but the effect of m_2 on

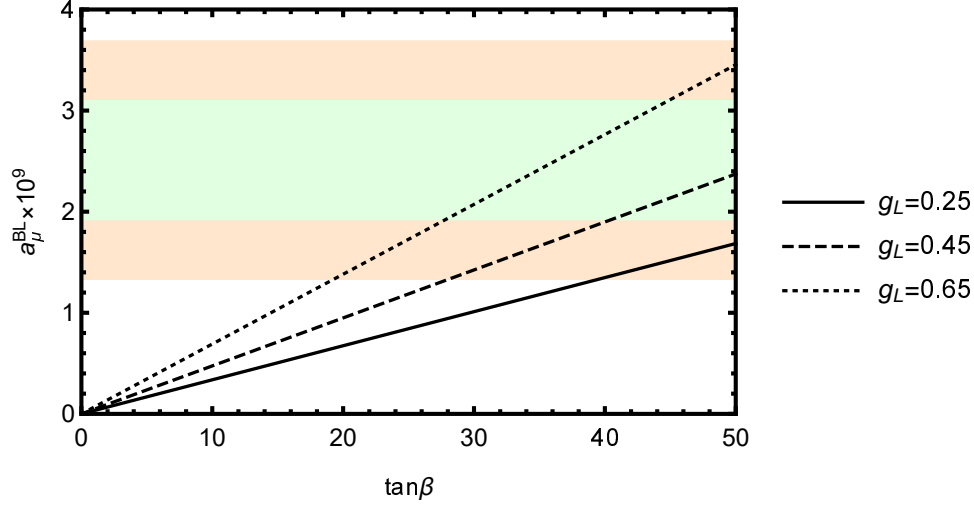


FIG. 7: The BLMSSM contributions to muon MDM (a_μ^{BL}) versus $\tan\beta$.

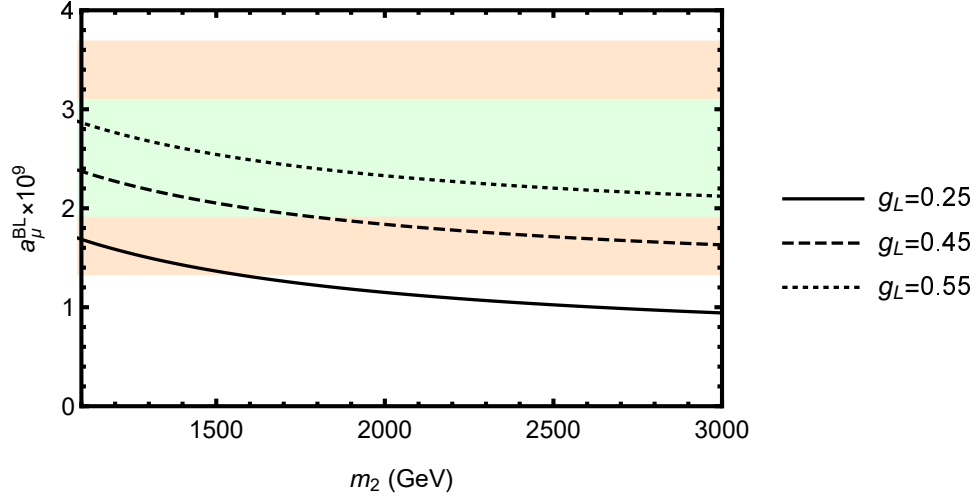


FIG. 8: The BLMSSM contributions to muon MDM (a_μ^{BL}) versus m_2 .

the function is considerable and inversely proportional in Eqs. (22), (24) obtained by MIA. On the whole, the increase of m_2 leads to the slow decrease of a_μ^{BL} . The dotted and dashed lines are all located in the colored areas. The dotted line can reach 2.9×10^{-9} , the dashed line can reach 2.4×10^{-9} and the solid line can reach 1.7×10^{-9} .

In addition, supposing the parameters with $g_L = 0.45$ and $m_2 = 1100$ GeV, we study the parameter μ_H influences on muon MDM in Fig. 9. μ_H is SUSY invariant Higgs mass, which exists in each contribution of Fig. 3. The solid line, dashed line and dotted line respectively correspond to the results with $\tan\beta = 30$, $\tan\beta = 40$ and $\tan\beta = 50$. All three lines have a slight positive slope. Among the dominant terms, $a_\mu^{BL,(a)}$, $a_\mu^{BL,(e)}$, and $a_\mu^{BL,(f)}$

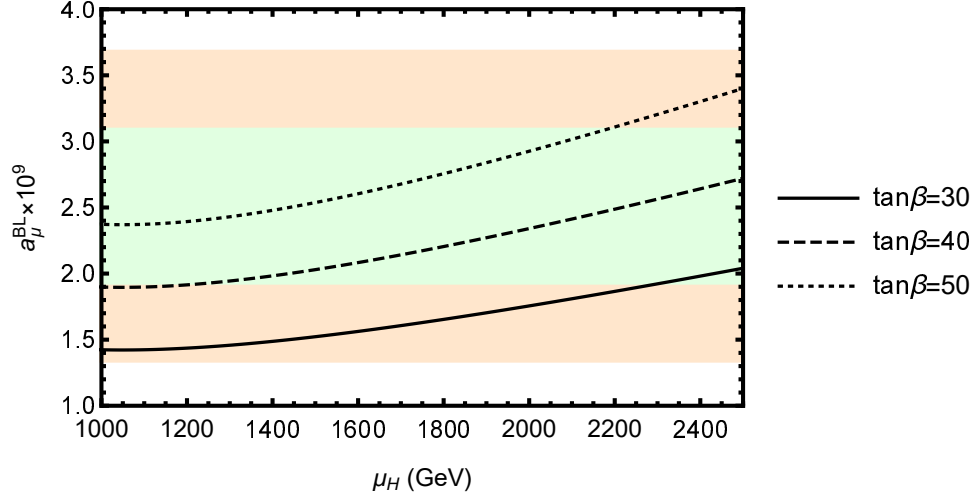


FIG. 9: The BLMSSM contributions to muon MDM (a_μ^{BL}) versus μ_H .

are proportional to $\sqrt{x_{\mu_H}} = \frac{m_{\mu_H}}{M_{SUSY}}$, but the function parts are inversely proportional to μ_H and have a relatively small effect. After combination, the effect of μ_H on muon MDM shows a slowly increasing relationship, when μ_H increases from 1000 GeV to 2500 GeV. The three curves all are in the colored areas, which mean that a_μ^{BL} satisfies the experimental limitations under our assumption. The dotted line is at the top, that is, large $\tan \beta$ value results in larger a_μ^{BL} . All three lines can exceed 2.0×10^{-9} .

2. Multidimensional scatter plots graphs

In this part, we carry out numerical analysis by scanning free parameters and explore the region to explain the BLMSSM contributions to muon MDM. The random ranges of input parameters are as follows:

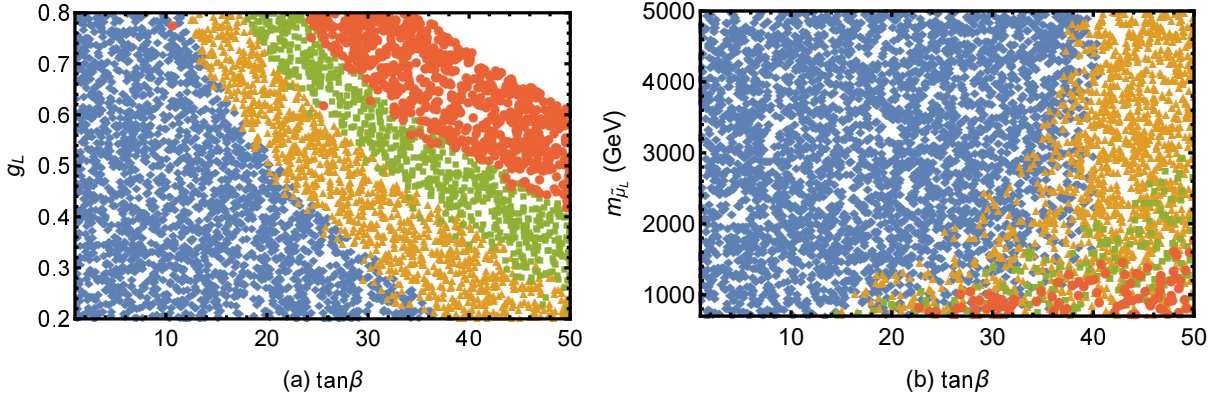
$$\begin{aligned} \tan \beta &\supset [1, 50], \quad g_L \supset [0.2, 0.8], \quad m_1 \supset [100, 3000] \text{ GeV}, \\ m_2 &\supset [1000, 3000] \text{ GeV}, \quad \mu_H \supset [1000, 3000] \text{ GeV}, \quad m_{\tilde{\nu}_L} \supset [100, 3000] \text{ GeV}, \\ m_{\tilde{\mu}_L} &\supset [700, 3000] \text{ GeV}, \quad m_{\tilde{\mu}_R} \supset [700, 3000] \text{ GeV}, \quad |m_L| \supset [200, 5000] \text{ GeV}. \end{aligned} \quad (37)$$

In Table II, we show the markers for Figs. 10–12.

To better display sensitive parameters, we show the a_μ^{BL} in the $\tan \beta - g_L$ plane (a) and $\tan \beta - m_{\tilde{\mu}_L}$ plane (b) in Fig. 10. The bounds between \blacklozenge , \blacktriangle , \blacksquare and \bullet are very obvious in Fig. 10(a). The blue part is displayed in a trapezoid and takes up a lot of space. The

TABLE II: The meaning of shape style

Shape style	Figs. 10,11	Fig. 12
◆	$0 < a_\mu^{BL} < 10^{-9}$	$0 < a_\mu^{BL} < 1.5 \times 10^{-9}$
▲	$10^{-9} \leq a_\mu^{BL} < 1.5 \times 10^{-9}$	$1.5 \times 10^{-9} \leq a_\mu^{BL} < 2.0 \times 10^{-9}$
■	$1.5 \times 10^{-9} \leq a_\mu^{BL} < 2.0 \times 10^{-9}$	$2.0 \times 10^{-9} \leq a_\mu^{BL} < 3.0 \times 10^{-9}$
●	$2.0 \times 10^{-9} \leq a_\mu^{BL} < 3.0 \times 10^{-9}$	\


 FIG. 10: a_μ^{BL} in $\tan \beta - g_L$ plane (a) and $\tan \beta - m_{\tilde{\mu}_L}$ plane (b).

results represented by the remaining three colors show a slight radian. The red part is on the upper right corner, that is, large $\tan \beta$ and large g_L can bring greater contributions. Similarly, ◆ also occupy a large number of positions in Fig. 10(b) and mainly in the wide area $1 < \tan \beta < 40$ and $700 \text{ GeV} < m_{\tilde{\mu}_L} < 5000 \text{ GeV}$. ● concentrate in the narrow area $\tan \beta$ (22, 50) and $m_{\tilde{\mu}_L}$ (700, 1600) GeV. $m_{\tilde{\mu}_L}$ is left-handed smuon mass. The function parts of $a_\mu^{BL,(a)}$, $a_\mu^{BL,(c)}$, $a_\mu^{BL,(d)}$, and $a_\mu^{BL,(e)}$ are inversely proportional to $m_{\tilde{\mu}_L}$. Therefore, this means that light scalar muon improves the BLMSSM contributions to muon MDM.

We plot a_μ^{BL} in the plane of $m_{\tilde{\nu}_L}$ versus $|m_L|$ by the left diagram in the Fig. 11, and the right diagram shows the relation between a_μ^{BL} , $m_{\tilde{\nu}_L}$ and g_L . One can find that the styles of Fig. 11(a) and Fig. 10(b) are similar. In Fig. 11(a), the blue area is the most. In the range $800 \text{ GeV} < |m_L| < 1200 \text{ GeV}$, ▲ occupy much space. ■ concentrate in the narrow area $|m_L| < 800 \text{ GeV}$ and $1500 \text{ GeV} < m_{\tilde{\nu}_L} < 3000 \text{ GeV}$. ● denote large contributions to a_μ^{BL} that are concentrate in the area $|m_L| < 1000 \text{ GeV}$ and $100 \text{ GeV} < m_{\tilde{\nu}_L} < 1500 \text{ GeV}$. m_L expresses the mass of new gaugino λ_L beyond MSSM. We take m_L as a negative value in the Eq. (23) and can easily find that this contribution is proportional to $\sqrt{x_L} = \frac{m_L}{M_{SUSY}}$.

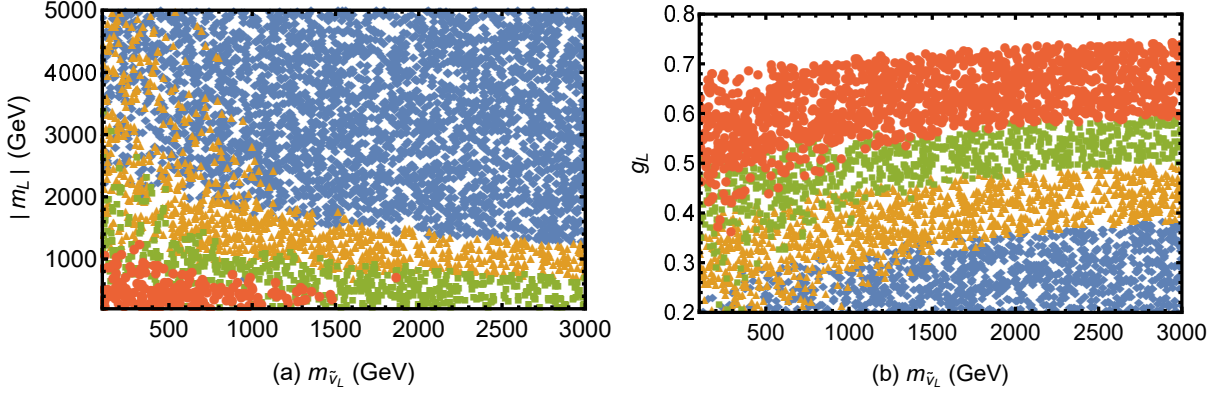


FIG. 11: a_μ^{BL} in $m_{\tilde{\nu}_L} - |m_L|$ plane (a) and $m_{\tilde{\nu}_L} - g_L$ plane (b).

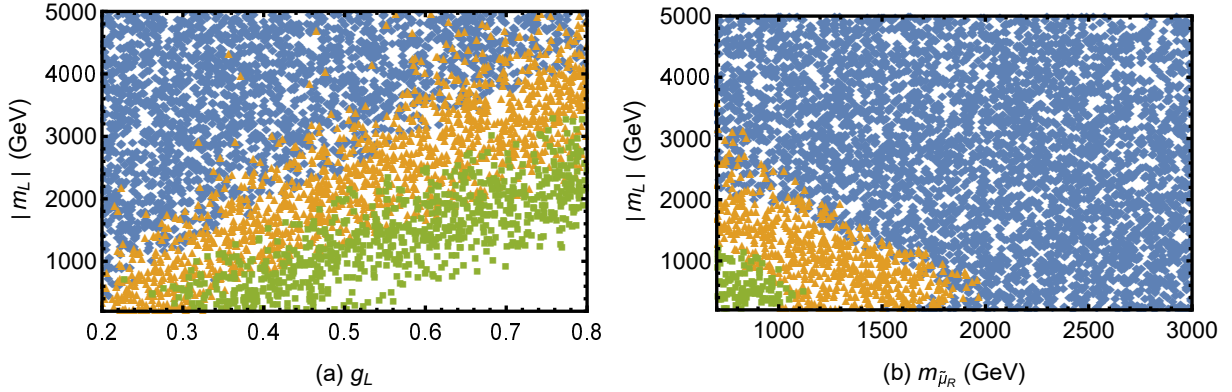


FIG. 12: a_μ^{BL} in $g_L - |m_L|$ plane (a) and $m_{\tilde{\mu}_R} - |m_L|$ plane (b).

For more convenience, we take $|m_L|$ as the ordinate. These indicate that small $|m_L|$ and small $m_{\tilde{\nu}_L}$ can lead to large corrections. In Fig. 11(b), the layers are distinct, with \blacktriangle , \blacksquare and \bullet arched. In the case of $m_{\tilde{\nu}_L} = 3000$ GeV, we can find these laws. When $g_L < 0.38$, the space is filled with \blacklozenge . The red, green and blue parts correspond to $0.38 < g_L < 0.5$, $0.5 < g_L < 0.6$ and $0.6 < g_L < 0.74$, respectively. $m_{\tilde{\nu}_L}$ denotes the mass of the left-handed neutrino, which causes a change in $a_\mu^{BL,(f)}$ by directly affecting the function part of Eq. (24). The final effect is that a_μ^{BL} is inversely proportional to $m_{\tilde{\nu}_L}$. In the whole, small $m_{\tilde{\nu}_L}$ and large g_L can obviously improve the corrections to a_μ^{BL} .

Furthermore, we show the relationship between g_L and $|m_L|$, $m_{\tilde{\mu}_R}$ and $|m_L|$ in Fig. 12. It is worth noting that the meanings of \blacklozenge , \blacktriangle and \blacksquare in Fig. 12 are inconsistent with those in Figs. 10,11. The specific meanings are shown in right part of Table II. The left figure and the right figure have obvious stratification and strong regularity. In Fig. 12(a), the

results are divided into two parts by the diagonal. \blacklozenge concentrate in the upper left of the diagonal and \blacktriangle and \blacksquare mainly distribute at the bottom right of the diagonal. In Fig. 12(b), the whole space is covered. \blacksquare concentrate in the narrow area $m_{\tilde{\mu}_R}$ (700, 1000) GeV and $|m_L|$ (200, 1000) GeV. \blacktriangle occupy much space in the range 700 GeV < $|m_L|$ < 2000 GeV and 1000 GeV < $m_{\tilde{\mu}_R}$ < 1800 GeV. The blue part occupies all the remaining positions. $m_{\tilde{\mu}_R}$ is right-handed smuon mass. Only the function parts of $a_\mu^{BL,(a)}$, $a_\mu^{BL,(b)}$ and $a_\mu^{BL,(e)}$ contain $m_{\tilde{\mu}_R}$ and are inversely proportional to $m_{\tilde{\mu}_R}$. The results imply that large $m_{\tilde{\mu}_R}$ and large $|m_L|$ can diminish the BLMSSM contributions to muon MDM. Based on the above description, we can be more clear about the contribution of the above parameters.

C. The lepton EDM by MIA

In this subsection, we research and analyze the one-loop contributions of the lepton (e, μ, τ) EDM in the frame work of CP violating BLMSSM via the mass insertion approximation. According to Part B of Section III, d_l^{BL} mainly depends on 15 parameters, i.e., $\tan\beta$, g_L , M_1 , M_2 , M_L , M_{μ_H} , M_{μ_L} , $m_{\tilde{\nu}_L}$, $m_{\tilde{L}_R}$, $m_{\tilde{L}_L}$, θ_1 , θ_2 , θ_{μ_H} , θ_{μ_L} and θ_L . We take these parameters as free parameters and calculate the BLMSSM contributions to the lepton (e, μ, τ) EDM for a given set of parameters, and fix the parameter $M_{SUSY} = 1000$ GeV.

1. The electron EDM

First of all, we discuss the electron EDM because its experimental upper limit is very strict. The analysis consists of three parts: 1. make the CP violating phases small $O(10^{-2} - 10^{-3})$; 2. increase the particle mass to the several 10 TeV range; 3. make internal cancellations between phases. The light green areas of Figs. 13,14,15 represent the experimental limitations of electron EDM.

a. Small phases

Supposing $M_1 = 800$ GeV, $M_2 = 1100$ GeV, $M_L = -3000$ GeV, $M_{\mu_H} = 1100$ GeV, $M_{\mu_L} = 1100$ GeV, $m_{\tilde{\nu}_L} = 300$ GeV, $m_{\tilde{L}_R} = 1800$ GeV, $m_{\tilde{L}_L} = 1800$ GeV, $\theta_1 = \theta_2 = \theta_{\mu_H} = \theta_L = 0$ and $\theta_{\mu_L} = \pi/1000$, we study the contributions from g_L to electron EDM. We plot the solid line, dashed line and dotted line versus $g_L(0 - 0.8)$ corresponding to $\tan\beta = (8, 10, 12)$ in Fig. 13. Obviously, these three lines are all increasing functions of g_L . With $\tan\beta =$

12, $\tan\beta = 10$ and $\tan\beta = 8$, d_e^{BL} can satisfy the experimental bound in the g_L region $(0 - 0.45)$, $(0 - 0.5)$ and $(0 - 0.6)$, respectively. Therefore, a small phase and particle mass in the TeV range can satisfy the experimental constraints of electron EDM. However, a small phase represents fine tuning unless it occurs naturally, for example as a loop correction.

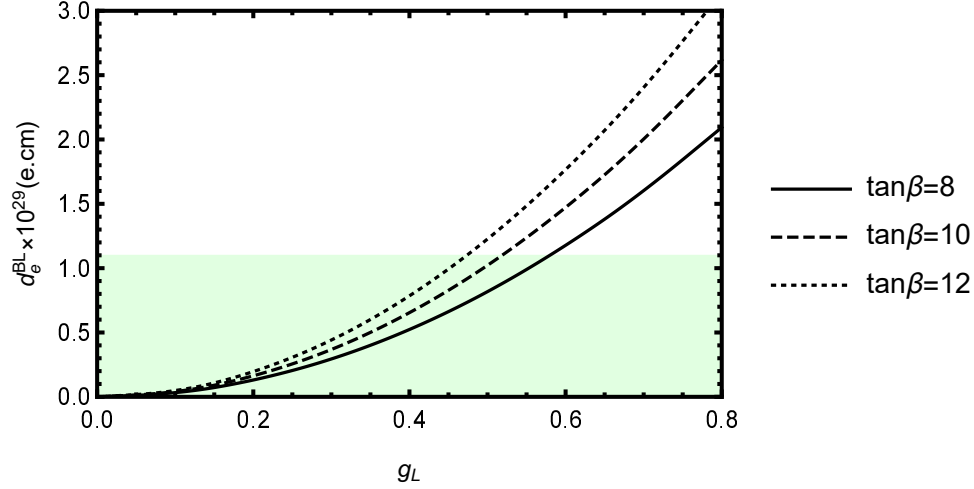


FIG. 13: With $\theta_{\mu_L} = \pi/1000$, and $\theta_1 = \theta_2 = \theta_{\mu_H} = \theta_L = 0$, the BLSSM contributions to electron EDM (d_e^{BL}) versus g_L .

b. Mass suppression

The parameters $g_L = 0.1$, $M_1 = 800$ GeV, $M_2 = 1100$ GeV, $M_L = 4500$ GeV, $M_{\mu_H} = 1100$ GeV, $m_{\tilde{\nu}_L} = 300$ GeV, and $\theta_1 = \theta_2 = \theta_{\mu_H} = \theta_L = 0$ are adopted. The remaining parameters are large masses of particles, i.e., $M_{\mu_L} = 30000$ GeV, $m_{\tilde{L}_R} = 40000$ GeV and $m_{\tilde{L}_L} = 40000$ GeV. With $\tan\beta = (10, 15, 20)$, the results are shown by the solid line, dashed line and dotted line respectively in Fig. 14. θ_{μ_L} is the CP violating phase of new parameter μ_L . μ_L relates with sneutrino mass squared matrix and lepton neutralino mass matrix. The shapes of the three lines are consistent, and they are very similar as $-\sin\theta_{\mu_L}$. For θ_{μ_L} from π to 2π , the dotted line is up the dashed line and the dashed line is up the solid line. Total solid line and most parts of dashed and dotted lines are in the light green area. That is to say, particle mass in the several 10 TeV range and a normal phase can easily satisfy the experimental limitations of electron EDM. However, this violates the naturalness. Obviously, the several 10 TeV range even may be out of reach of LHC.

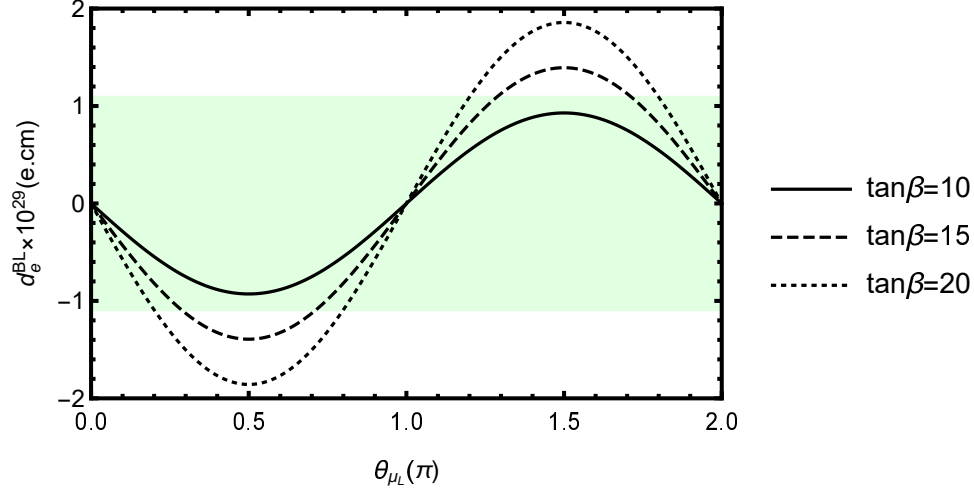


FIG. 14: With $\theta_1 = \theta_2 = \theta_{\mu_H} = \theta_L = 0$, the BLMSSM contributions to electron EDM (d_e^{BL}) versus θ_{μ_L} .

c. Internal cancellations

To sum up, we discuss the third possible method, which is internal cancellations among the different phases of the electron EDM. We study the numerical results versus Θ ($\Theta = \theta_{\mu_L} = \theta_{\mu_H}$) with $g_L = 0.5$, $M_1 = 800$ GeV, $M_2 = 2200$ GeV, $M_L = 1000$ GeV, $M_{\mu_H} = 1800$ GeV, $M_{\mu_L} = 1200$ GeV, $m_{\tilde{\nu}_L} = 1200$ GeV, $m_{\tilde{L}_R} = 700$ GeV, $m_{\tilde{L}_L} = 700$ GeV and $\theta_1 = \theta_2 = \theta_L = 0$. The corresponding results are plotted by the solid line, dashed line and dotted line in Fig. 15. The three lines all look like $\sin \Theta$. At these points $\Theta = 0$, $\Theta = \pi$, and $\Theta = 2\pi$, there is none CP violating effect and $d_e^{BL} = 0$ is reasonable. The largest values of the three lines are respectively 1.01×10^{-29} e.cm, 1.21×10^{-29} e.cm and 1.51×10^{-29} e.cm. With $\tan \beta = 10$, the solid line all in the experiment constraint. This possible method has normal size CP violating phases $O(1)$ and particle mass in the TeV range. The obtained results can also more easily satisfy the experimental limitations of electron EDM.

2. The muon EDM

At present, the experimental upper bound of muon EDM is $|d_\mu^{exp}| < 1.8 \times 10^{-19}$ e.cm. In the part, we adopt the parameters as $\tan \beta = 15$, $M_1 = 800$ GeV, $M_2 = 1100$ GeV, $M_{\mu_H} = 1100$ GeV, $M_{\mu_L} = 2500$ GeV, $m_{\tilde{\nu}_L} = 150$ GeV, $m_{\tilde{L}_R} = 700$ GeV, $m_{\tilde{L}_L} = 700$ GeV, $\theta_1 = \theta_2 = \theta_{\mu_H} = \theta_{\mu_L} = 0$ and $\theta_L = \pi/3$. We study d_μ^{BL} versus M_L with $g_L = (0.3, 0.4, 0.5)$, and

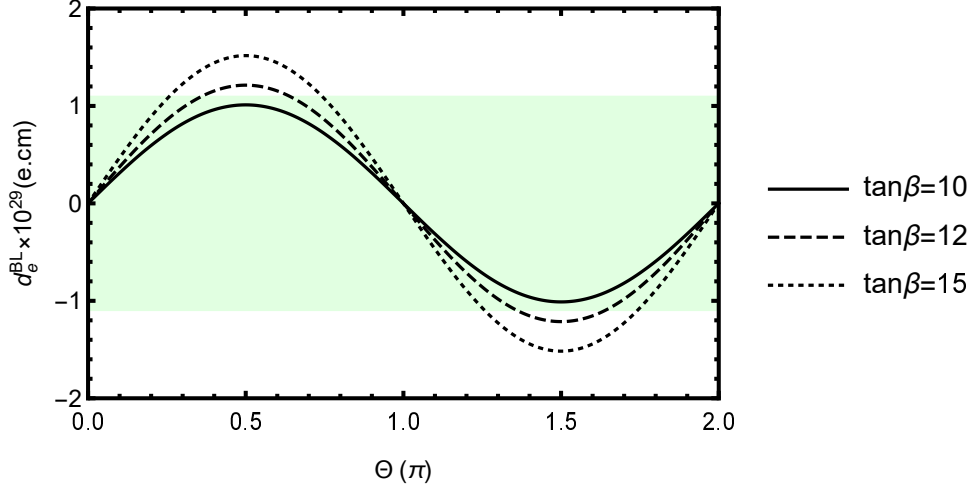


FIG. 15: With $\theta_1 = \theta_2 = \theta_L = 0$, the BLSSM contributions to electron EDM (d_e^{BL}) versus Θ ($\Theta = \theta_{\mu_L} = \theta_{\mu_H}$).

the results are plotted by the solid line, dashed line and dotted line in Fig. 16. M_L is the gaugino mass for the new gaugino λ_L . In Eq. (34), $d_l^{BL,(e)}$ is proportional to $\sqrt{x_L} = \frac{|M_L|}{M_{SUSY}}$. The dashed line reaches 2.38×10^{-23} e.cm as $M_L = -360$ GeV. When $|M_L| > 360$ GeV, the absolute values of the numerical results shrink with the enlarging $|M_L|$. Larger g_L results in larger d_μ^{BL} , when the other parameters are same. All numerical results are around the order of 10^{-22} e.cm, which is almost three-order smaller than muon EDM upper bound.

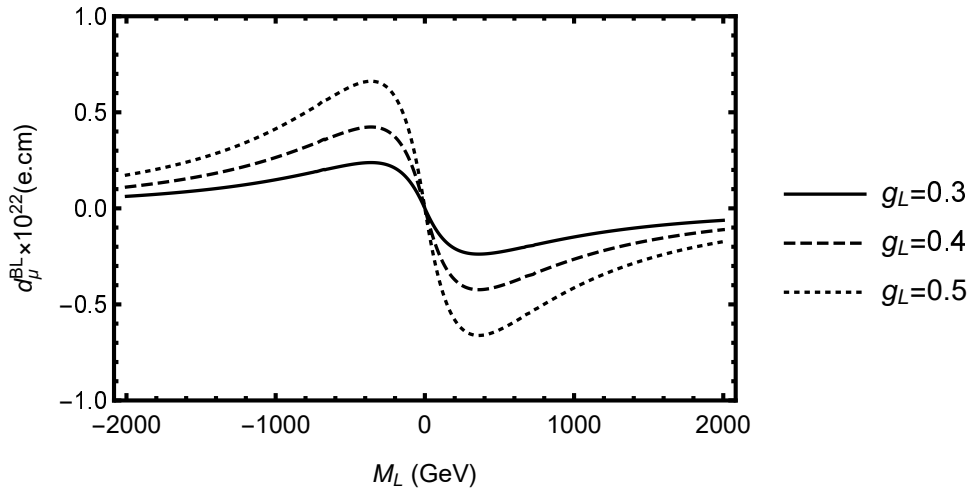


FIG. 16: With $\theta_L = \pi/3$, and $\theta_1 = \theta_2 = \theta_{\mu_H} = \theta_{\mu_L} = 0$, the BLSSM contributions to muon EDM (d_μ^{BL}) versus M_L .

3. The tau EDM

Among the lepton EDM bounds, the tau EDM has the loosest experimental upper limit, which is about 10^{-17} e.cm. Now, supposing $g_L = 0.6$, $M_1 = 800$ GeV, $M_2 = 1100$ GeV, $M_L = -500$ GeV, $M_{\mu_H} = 1100$ GeV, $M_{\mu_L} = 1100$ GeV, $m_{\tilde{\nu}_L} = 150$ GeV, $m_{\tilde{L}_R} = 1500$ GeV, $m_{\tilde{L}_L} = 1500$ GeV, and $\theta_1 = \theta_2 = \theta_{\mu_H} = \theta_L = 0$, we study the influence of θ_{μ_L} on tau EDM (d_τ^{BL}). In Fig. 17, the solid line, dashed line and dotted line respectively correspond to $\tan\beta = (10, 20, 30)$ and their numerical results are all within the experimental limits of tau EDM. There is none CP violating effect and $d_\tau^{BL} = 0$ is reasonable, as $\theta_{\mu_L} = 0$, $\theta_{\mu_L} = \pi$ and $\theta_{\mu_L} = 2\pi$. When $\theta_{\mu_L} = 0.5\pi$ and $\theta_{\mu_L} = 1.5\pi$, the absolute value of d_τ^{BL} reaches the maximum. The dotted line can arrive at 1.47×10^{-22} e.cm. Generally speaking, the results are about five-order smaller than the experimental bound of the tau EDM.

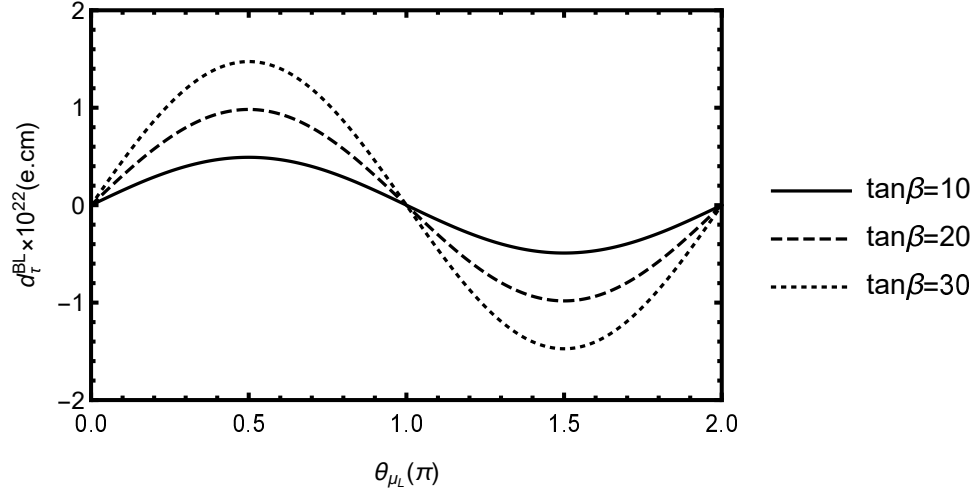


FIG. 17: With $\theta_1 = \theta_2 = \theta_{\mu_H} = \theta_L = 0$, the BLMSSM contributions to tau EDM (d_τ^{BL}) versus θ_{μ_L} .

V. DISCUSSION AND CONCLUSION

In the framework of the BLMSSM, we study the one-loop contributions to the muon MDM and the lepton (e, μ, τ) EDM. During the analysis, the mass insertion approximation is used to more clearly display sensitive parameters. All parameters used can satisfy the latest experimental data. The relative error ($\frac{ME-MIA}{ME}$) between the mass eigenstate (ME) and the mass insertion approximation (MIA) is about 1%, which is shown as a narrow area

in the figure. Therefore, the accuracy of the MIA expressions is verified.

As we mentioned before, there are dominant three parts on which a_μ^{BL} depends, i.e., $a_\mu^{BL,(a)}$, $a_\mu^{BL,(e)}$ and $a_\mu^{BL,(f)}$. We take $\tan\beta$, g_L , m_1 , m_2 , m_L , μ_H , $m_{\tilde{\nu}_L}$, $m_{\tilde{\mu}_R}$ and $m_{\tilde{\mu}_L}$ as free parameters. Among them, $\tan\beta$, g_L , m_L and μ_H are more sensitive parameters. a_μ^{BL} is an increasing function of $\tan\beta$, g_L , μ_H and decreasing function of m_2 . Small $|m_L|$ and small $m_{\tilde{\nu}}$ can improve the BLMSSM contributions to muon MDM. In our used parameter space, the contributions to muon MDM can easily reach its upper bound and even exceed it. Our best numerical result of a_μ^{BL} is around 2.5×10^{-9} , which can well compensate the departure between the experiment data and the SM prediction.

The effects of the CP violating phases $\theta_1, \theta_2, \theta_{\mu_H}, \theta_{\mu_L}, \theta_L$ on the lepton (e, μ, τ) EDM are researched. Using MIA, the impact of the CP violating phases on d_l^{BL} can be observed more intuitively. The addition of two new CP violating sources $(\theta_{\mu_L}, \theta_L)$ and the coupling constant g_L can enhance the one-loop contributions from the neutralino-slepton diagram by several orders. The upper bound of electron EDM is 1.1×10^{-29} e.cm, which is the most stringent. This poses a challenge to the BLMSSM parameter space. By using the method of two phases cancellation, the contributions to electron EDM can be controlled below the experimental limit in our parameter space. The numerical results of muon EDM and tau EDM are several orders smaller than their upper limits, and at the order of 10^{-22} e.cm in our used parameter space. With the improvement of technical accuracy, the lepton EDM may be detected by the experiments in the near future.

Acknowledgments

This work is supported by National Natural Science Foundation of China (NNSFC) (No.12075074), Natural Science Foundation of Hebei Province (A2020201002, A202201022, A2022201017), Natural Science Foundation of Hebei Education Department (QN2022173), Post-graduate's Innovation Fund Project of Hebei University (HBU2022ss028, HBU2023SS043), the youth top-notch talent support program of the Hebei Province.

-
- [1] T. Aoyama, N. Asmussen, M. Benayoun, et al., *Phys. Rept.* **887** (2020) 1.
 - [2] G.W. Bennett, et al., *Phys. Rev. D* **73** (2006) 072003.
 - [3] A. Keshavarzi, D. Nomura, T. Teubner, *Phys. Rev. D* **97** (2018) 114025.
 - [4] G. Colangelo, M. Hoferichter, P. Stoffer, *J. High Energy Phys.* **02** (2019) 006.
 - [5] M. Hoferichter, B.L. Hoid, B. Kubis, *J. High Energy Phys.* **08** (2019) 137.
 - [6] M. Davier, A. Hoecker, B. Malaescu, et al., *Eur. Phys. J. C.* **80** (2020) 241.
 - [7] A. Keshavarzi, D. Nomura, T. Teubner, *Phys. Rev. D* **101** (2020) 014029.
 - [8] T. Blum, P.A. Boyle, V. Gulpers, et al., *Phys. Rev. Lett.* **121** (2018) 022003.
 - [9] T. Aoyama, M. Hayakawa, T. Kinoshita, et al., *Phys. Rev. Lett.* **109** (2012) 111808.
 - [10] G. Colangelo, F. Hagelstein, M. Hoferichter, et al., *J. High Energy Phys.* **03** (2020) 101.
 - [11] G. Eichmann, C.S. Fischer, R. Williams, *Phys. Rev. D* **101** (2020) 054015.
 - [12] T. Blum, N. Christ, M. Hayakawa, et al., *Phys. Rev. Lett.* **124** (2020) 132002.
 - [13] T. Aoyama, T. Kinoshita, M. Nio, *Atoms* **7** (2019) 28.
 - [14] A. Czarnecki, W.J. Marciano, A. Vainshtein, *Phys. Rev. D* **67** (2003) 073006.
 - [15] C. Gnendiger, D. Stockinger, H.S. Kim, *Phys. Rev. D* **88** (2013) 053005.
 - [16] M.T. Hansen, A. Patella, *J. High Energy Phys.* **10** (2020) 029.
 - [17] H. Davoudiasl, W.J. Marciano, *Phys. Rev. D* **98** (2018) 075011.
 - [18] K. Hagiwara, A. Keshavarzi, A.D. Martin, et al., *Nucl. Part. Phys. Proc.* **287-288** (2017) 33-38.
 - [19] Muon g-2 Collaboration, *Phys. Rev. Lett.* **126** (2021) 141801.
 - [20] A. Shindler, *Eur. Phys. J. A.* **57** (2021) 128 .
 - [21] J. Baron, et al., (ACME Collaboration) *Science* **343** (2014) 269.
 - [22] V. Andreev, et al., (ACME Collaboration) *Nature* **562** (2018) 355-60.
 - [23] A. Crivellin, M. Hoferichter, P.S. Wellenburg, *Phys. Rev. D* **98** (2018) 113002.
 - [24] R.L. Workman, et al., (Particle Data Group), *Prog. Theor. Exp. Phys.* **2022** (2022) 083C01.
 - [25] M.E. Pospelov and I.B. Khriplovich, *Sov. J. Nucl. Phys.* **53** (1991) 638.
 - [26] M. Pospelov and A. Ritz, *Phys. Rev. D.* **89** (2014) 056006.
 - [27] S. Heinemeyer, D. Stöckinger, G. Weiglein, *Nucl. Phys. B* **690** (2004) 62.

- [28] S. Heinemeyer, D. Stöckinger, G. Weiglein, *Nucl. Phys. B* **699** (2004) 103.
- [29] F. Wang, L. Wu, Y. Xiao, et al., *Nucl. Phys. B.* **970** (2021) 115486 [arXiv:2104.03262].
- [30] J.J. Cao, J.W. Lian, Y.S. Pan, et al., *J. High Energy Phys.* **09** (2021) 175 [arXiv:2104.03284].
- [31] J.J. Cao, X.L. Jia, L. Meng, et al., [arXiv:2210.08769].
- [32] J.J. Cao, J.W. Lian, Y.S. Pan, et al., *J. High Energy Phys.* **03** (2022) 203 [arXiv:2201.11490].
- [33] J.J. Cao, F. Li, J.W. Lian, et al., *Sci.China Phys.Mech.Astron.* **65** (2022) 9, 291012 [arXiv:2204.04710].
- [34] W. Yin, *J. High Energy Phys.* **06** (2021) 029 [arXiv:2104.03259].
- [35] W. Yin, M. Yamaguchi, *Phys.Rev.D* **106** (2022) 3, 033007 [arXiv:2012.03928].
- [36] S.M. Zhao, T.F. Feng, H.B. Zhang, et al., *J. High Energy Phys.* **11** (2014) 119 [arXiv:1405.7561].
- [37] J.L. Yang, H.B. Zhang, C.X. Liu, et al., *J. High Energy Phys.* **08** (2021) 086.
- [38] J.L. Yang, T.F. Feng, Y.L. Yan, et al., *Phys. Rev. D.* **99** (2019) 015002.
- [39] L.H. Su, S.M. Zhao, X.X. Dong, et al., *Eur. Phys. J. C* **81** (2021) 433.
- [40] S.M. Zhao, L.H. Su, and X.X. Dong, et al., *J. High Energy Phys.* **03** (2022) 101.
- [41] C.X. Liu, H.B. Zhang, J.L. Yang, et al., *J. High Energy Phys.* **04** (2020) 002.
- [42] F. del Aguila, M. B. Gavela, J. A. Grifols, et al., *Phys. Lett. B* **129** (1983) 473.
- [43] T. Ibrahim, P. Nath, *Phys. Rev. D* **60** (1999) 099902.
- [44] S. Atag, E. Gurkanli, *J. High Energy Phys.* **1606** (2016) 118.
- [45] T. Abe, N. Omoto, O. Seto, et al., *Phys. Rev. D* **98** (2018) 075029.
- [46] J. Rosiek, *Phys. Rev. D* **41** (1990) 3464.
- [47] H.P. Nilles, *Phys. Rept.* **110** (1984) 1.
- [48] H.E. Haber, G.L. Kane, *Phys. Rept.* **117** (1985) 75.
- [49] S.M. Zhao, T.F. Feng, X.J. Zhan, et al., *J. High Energy Phys.* **07** (2015) 124.
- [50] T. Ibrahim and P. Nath, *Phys. Rev. D* **57** (1998) 478.
- [51] T. Ibrahim and P. Nath, *Phys. Rev. D* **58**(1998) 019901.
- [52] P.F. Perez and M.B. Wise, *J. High Energy Phys.* **08** (2011) 068.
- [53] P.F. Perez and M.B. Wise, *Phys. Rev. D* **82** (2010) 011901.
- [54] P.F. Perez, *Phys. Rept.* **597** (2015) 1-30.
- [55] P.F. Perez, *Phys. Lett. B* **711** (2012) 353 [arXiv:1201.1501].
- [56] J.M. Arnold, P.F. Perez, B. Fornal, et al., *Phys. Rev. D* **85** (2012) 115024 [arXiv:1204.4458].

- [57] T.F. Feng, S.M. Zhao, H.B. Zhang, et al., *Nucl. Phys. B* **871** (2013) 223.
- [58] E. Arganda, M.J. Herrero, R. Morales, et al., *J. High Energy Phys.* **03** (2016) 055.
- [59] T.F. Feng, L. Sun, X.Y. Yang, *Nucl. Phys. B* **800** (2008) 221-252.
- [60] T. Moroi, *Phys. Rev. D* **53** (1996) 6565-6575.
- [61] D. Stockinger, *J. Phys. G* **34** (2007) R45-R92.
- [62] P. Athron, C. Balazs, D.H.J. Jacob, et al., *J. High Energy Phys.* **09** (2021) 080 [arXiv:2104.03691].
- [63] M. Endo, K. Hamaguchi, S. Iwamoto, et al., *J. High Energy Phys.* **07** (2021) 075.
- [64] M. Chakraborti, L. Roszkowski and S. Trojanowski, *J. High Energy Phys.* **05** (2021) 252 [arXiv:2104.04458].
- [65] P. Cox, C.C. Han, and T.T. Yanagida, *Phys. Rev. D.* **104** (2021) 075035 [arXiv:2104.03290].
- [66] M.V. Beekveld, W. Beenakker, M. Schutten, et al., *SciPost Phys.* **11** (2021) 3, 049 [arXiv:2104.03245].
- [67] M. Chakraborti, S. Heinemeyer and I. Saha, *Eur. Phys. J. C.* **81** (2021) 12, 1114 [arXiv:2104.03287].
- [68] CMS Collaboration, *Phys. Lett. B* **716** (2012) 30.
- [69] ATLAS Collaboration, *Phys. Lett. B* **716** (2012) 1.
- [70] ATLAS Collaboration, *Phys. Lett. B* **796** (2019) 68 [arXiv:1903.06248].